

1 **Glaciers determine the sensitivity of hydrological processes to perturbed climate**
2 **in a large mountainous basin on the Tibetan Plateau**

3
4 **Yi Nan ¹, Fuqiang Tian ¹**

5 **Affiliation:**

6 1. State Key Laboratory of Hydrosience and Engineering & Department of Hydraulic
7 Engineering, Tsinghua University, Beijing 100084, China

8
9 **Corresponding to:** Fuqiang Tian

10 Email: tianfq@tsinghua.edu.cn

11
12 **Abstract**

13 The major rivers on the Tibetan Plateau supply important freshwater resources to riparian
14 regions, but are undergoing significant climate change in recent decades. Understanding the
15 sensitivities of hydrological processes to climate change is important for water resource
16 management, but large divergences exist in previous studies because of the uncertainties of
17 hydrological models and climate projection data. Meanwhile, the spatial pattern of local
18 hydrological sensitivities was poorly explored despite the strong heterogeneity on the Tibetan
19 Plateau. This study adopted the climate perturbation method to analyze the hydrological
20 sensitivities of a typical large mountainous basin (Yarlung Tsangpo River, YTR) to climate
21 change. We utilized the tracer-aided hydrological model Tsinghua Representative Elementary
22 Watershed-Tracer-aided version (THREW-T) to simulate the hydrological and cryospheric
23 processes in the YTR basin. Multiple datasets and internal stations were used to validate the
24 model, to provide confidence to the baseline simulation and the sensitivity analysis. Results
25 indicated that: (1) The THREW-T model performed well on simulating the streamflow, snow
26 cover area (SCA), glacier mass balance (GMB), and stream water isotope, ensuring good
27 representation of the key cryospheric processes and a reasonable estimation of runoff
28 components. The model performed acceptably on simulating the streamflow at eight internal
29 stations located in the mainstream and two major tributaries, indicating that the spatial pattern

30 of hydrological processes was reflected by the model. (2) Increasing temperature led to
31 decreasing annual runoff, smaller inter-annual variation, more even intra-annual distribution,
32 and an earlier maximum runoff. It also influenced the runoff regime by increasing the
33 contributions of rainfall and glacier melt overland runoff, but decreasing the subsurface runoff
34 and snowmelt overland runoff. Increasing precipitation had the opposite effect to increasing
35 temperature. (3) The local runoff change in response to increasing temperature varied
36 significantly, with changing rate of -18.6% to 54.3% for 5°C of warming. The glacier area ratio
37 (GAR) was the dominant factor of the spatial pattern of hydrological sensitivities to both
38 perturbed temperature and precipitation. Some regions had a non-monotonic runoff change rate
39 in response to climate perturbation, which represented the most dynamic regions within the
40 basin, as they kept shifting between energy and water limited stages. The GAR and mean annual
41 precipitation (MAP) of the non-monotonic regions had a linear relation, and formed the
42 boundary of regions with different runoff trends in the GAR-MAP plot.

43

44 **1. Introduction**

45 The Tibetan Plateau (TP), known as the “Asian Water Tower”, is the source region of
46 several major rivers in Asia (e.g., Yarlung Tsangpo-Brahmaputra Lantsang-Mekong, Indus,
47 Ganges). The contributions of runoff in the source regions of TP rivers to the total runoff in
48 whole basins range from 6%-60% (Tang et al., 2019; Wang et al., 2020; Cao and Pan, 2014),
49 sustaining the ecosystems and supplying valuable freshwater resources for downstream
50 livelihoods (Immerzeel et al., 2010; Lutz et al., 2014). The sustainable socioeconomic
51 development and the decision-making of water resource management in the riparian countries
52 around the TP rely heavily on the runoff in the major river basins (Cui et al., 2023). Meanwhile,
53 the TP is a typical high mountainous cryosphere, characterized by large stores of frozen soil
54 and frequent multiphase water transferring, resulting in complex hydrological processes and
55 multiple water sources including rainfall, snowmelt and glacier melt (Li et al., 2019; Yao et al.,
56 2022). The melting processes of frozen water are determined by energy budget, and the runoff
57 change on the TP is extremely sensitive to climate change (Gao et al., 2019). Consequently,
58 understanding hydrological processes and estimating the runoff change on the TP is not only of
59 great practical significance, but also a frontier scientific question in global change.

60 The TP is undergoing significant climate change in recent decades, with a warming rate
61 twice the global average level (Yao, 2019). Based on the recently released Coupled Model
62 Intercomparison Project Phase 6 (CMIP6) (Eyring et al., 2016), the warming levels of 1.5°C,
63 2°C and 3°C over the TP will be attained around the 2030s, 2050s and 2070s, respectively, and
64 the precipitation is also likely to increase significantly (Cui et al., 2023). The hydrological
65 cycling and water resources will change correspondingly; thus it is important to understand the
66 hydrological processes on the TP and the hydrological response to climate change. Plenty of
67 studies have adopted hydrological models to project the runoff change on the TP in the future,
68 but the reported trends and changing rates varied considerably in existing studies. Wang et al.
69 (2021) and Lutz et al. (2014) projected an increasing runoff trend till the end of 21st century,
70 while Cui et al. (2023) predicted the runoff to decrease before the 2030s and turn over to an
71 increasing trend after that. A primary reason for the divergence in existing studies is the model
72 uncertainties. The parameters are usually inadequately constrained solely by the streamflow
73 observation data because of the complex hydrological processes, resulting in large uncertainties

74 in the estimation on the contributions of runoff components (Tian et al., 2020; Nan et al., 2021a),
75 which influence the runoff projection significantly. For instance, Lutz et al. (2014) estimated
76 the contribution of glacier melt to annual runoff as 0.86~40.59% in the major TP rivers,
77 resulting in an increasing runoff with climate warming, while Cui et al. (2023) estimated the
78 contribution as 0.73~14.33% and resulting in a decreasing trend in the near future. Nonetheless,
79 recently developed hydrological models integrating key cryospheric processes (e.g., Cui et al.,
80 2023) have been proved as effective tools for hydrological simulations on the TP, and the high-
81 quality datasets of snow and glacier (e.g., Chen et al., 2018; Hugonnet et al., 2022) can provide
82 adequate validation for the corresponding models. Moreover, tracer-aided hydrological models
83 integrating modules of tracer storage, mixture, and transportation processes forced by the
84 outputs of isotopic general circulation models (iGCMs) have proved to constrain the
85 hydrological model uncertainties significantly (He et al., 2019; Birkel and Soulsby, 2015;
86 Stadnyk and Holmes, 2023), especially for the separation of runoff components (Nan et al.,
87 2021a, 2023). These developments of models and datasets bear the potential to provide a more
88 reasonable baseline for streamflow projection.

89 Another major source of runoff projection uncertainty is the uncertainty of climatic forcing
90 data (Li et al., 2014). The climatic data in the future are generally generated by the general
91 circulation models (GCMs), which cannot be directly adopted in the catchment scale because
92 of the insufficient spatial resolution and accuracy, so downscaling and bias correction are
93 necessary steps in using GCM data at regional scale (Xu et al., 2019; Olsson et al., 2015).
94 However, even being corrected by the observation data during the historical period, the
95 divergence among the outputs of different GCMs is still significant. For example, the difference
96 in the precipitation change over the TP among 22 CMIP6 products could be larger than 50%
97 (Cui et al., 2023). Bloschl and Montanari (2010) pointed out the large uncertainties of studies
98 analyzing the impact of climate change, and compared them to throwing a dice. As an
99 alternative method, producing hypothesized climate change scenarios by perturbing the current
100 temperature and precipitation data has proved to be valuable in investigating the hydrological
101 sensitivities to climate change (Ayguen et al., 2020; Rasouli et al., 2015; He et al., 2021b). The
102 range of climate perturbation is assumed based on the possible change range projected by an
103 ensemble of GCMs, providing a possible runoff change range accordingly (Su et al., 2023; He

104 et al., 2021b). The climate perturbation method also allows for a deeper analysis of the separate
105 effect of each climatic factor and the compensation effects among them (He and Pomeroy,
106 2023).

107 Although plenty of studies have been conducted for the TP rivers to project the runoff
108 change or analyze the hydrological sensitivities to climate change, most of them were
109 conducted at the regional or basin scale (e.g., Su et al., 2023; Zhang et al., 2022b). The local
110 hydrological response to climate change could significantly differ among small catchments due
111 to the different geographical and meteorological characteristics (Bai et al., 2023), which is
112 important for local water resources utilization and management (Zhang et al., 2015).
113 Considering the strong heterogeneity in meteorological factors and land surface conditions in
114 the large river basins on the TP (Wang et al., 2021; Li et al., 2020), the local hydrological
115 sensitivities to climate change should have strong variability over the TP. However, the spatial
116 pattern and influence factors of the local hydrological sensitivities within the basin are poorly
117 explored, partly due to the scarce hydrological stations for model validation, resulting in a lack
118 of confidence in the spatial representation of hydrological processes.

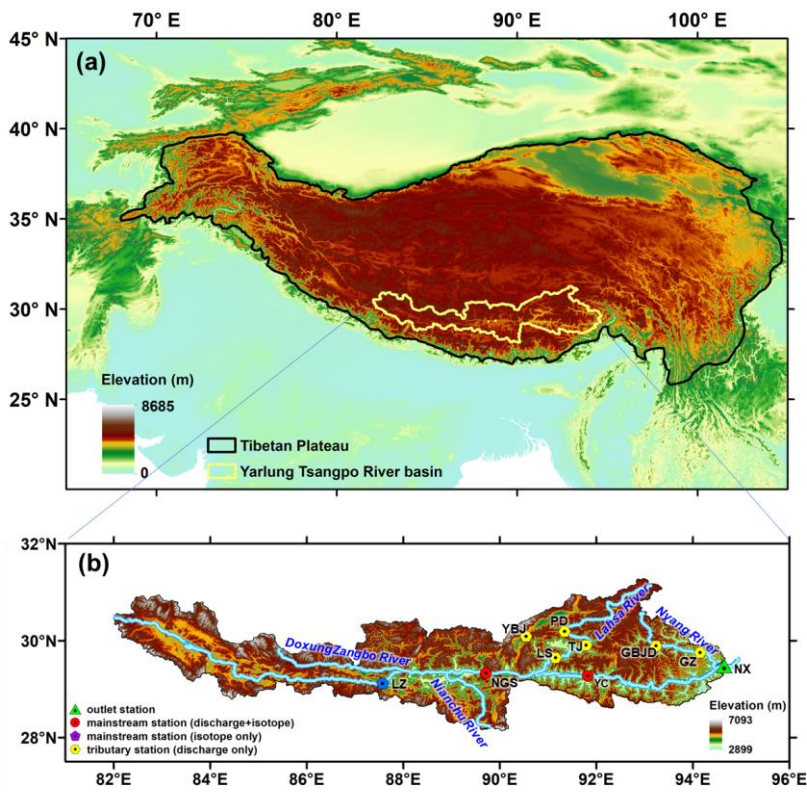
119 Motivated by the mentioned background, this study utilized the spatially distributed tracer-
120 aided hydrological model THREW-T developed by Nan et al. (2021b) in the Yarlung Tsangpo
121 River basin, a typical large mountainous basin on the Tibetan Plateau, to explore its
122 hydrological sensitivity to perturbed temperature and precipitation. Snow, glacier, isotope data
123 and observation streamflow at nine stations were collected to validate the model. The spatial
124 pattern of the local hydrological sensitivities and the influence factors were analyzed in
125 particular. The main objectives of this study are as follows: (1) to test the performance of
126 THREW-T model on simulating all the hydrological and cryospheric processes in the Yarlung
127 Tsangpo River basin, (2) to analyze the sensitivities of hydrological processes in the Yarlung
128 Tsangpo River basin to a reasonable range of perturbed temperature and precipitation, and (3)
129 to analyze the spatial pattern and the influence factors of the local hydrological sensitivities.

130 **2. Data and methodology**

131 **2.1 Study area**

132 This study focused on the Yarlung Tsangpo River (YTR) basin, the upstream part of the

133 Brahmaputra River basin, located in the southern TP (Figure 1). The YTR is one of the longest
 134 rivers originating from the TP (longer than 2000 km), extending in the range of 27~32°N and
 135 82~97°E with an elevation extent of 2900~6900 m a.s.l. (above sea level). The mean annual
 136 precipitation and temperature in the YTR basin are around 500 mm and -0.2 °C, respectively.
 137 The YTR has four major tributaries, i.e., DoxungZangbo, Nianchu River, Lhasa River, and
 138 Nyang River, from upstream to downstream. The precipitation is dominated by the South Asian
 139 monsoon in the Indian Ocean hydrosphere-atmosphere system, resulting in an obviously wet
 140 wet season from June to September. The outlet hydrological station along the mainstream is the
 141 Nuxia station, above which the drainage area is approximately 2×10^5 km², and around 1.5% is
 142 covered by glaciers.



143
 144 **Figure 1.** Locations and topography of (a) the Tibetan Plateau and (b) the Yarlung Tsangpo
 145 River basin. The stations used for model validation are shown in Figure (b). The abbreviations

146 NX, YC, NGS, LZ, GZ, GBJD, LS, TJ, PD and YBJ represent Nuxia, Yangcun, Nugesha, Lazi,
147 Gengzhang, Gongbujiangda, Lahsa, Tangjia, Pangduo and Yangbajing stations, respectively.

148 2.2 Data

149 The 30 m resolution digital elevation model (DEM) data for the YTR basin was extracted
150 from the Geospatial Data Cloud (<https://www.gscloud.cn>). Daily precipitation, temperature,
151 and potential evapotranspiration data were extracted from the China Meteorological Forcing
152 Dataset (CMFD, Yang and He, 2019) with 0.1° resolution. For the cryospheric processes, the
153 Tibetan Plateau Snow Cover Extent (TPSCE) product (Chen et al., 2018) and the second glacier
154 inventory dataset of China (Liu, 2012) were adopted to denote the snow and glacier coverage.
155 The yearly glacier elevation change data with 0.5° resolution developed by Hugonnet et al.
156 (2021) was used to represent the glacier mass balance. For the underlying conditions, the
157 MODIS leaf area index (LAI) product MOD15A2H (Myneni et al., 2015) and normalized
158 difference vegetation index (NDVI) product MOD13A3 (Didan, 2015) were adopted to
159 represent the vegetation coverages, and the Harmonized World Soil Database (HWSD, He,
160 2019) was used to estimate the soil property parameters. Daily streamflow data at nine stations
161 were collected (Figure 1 and Table 1).

162 **Table 1.** The name, location and data period of the hydrological stations

Station	Mainstream/tributary	Period
Nuxia	Mainstream	1991~2015
Yangcun	Mainstream	2001~2010
Nugesha	Mainstream	2001~2010
Gengzhang	Nyang river	2001~2015
Lhasa	Lhasa river	2001~2015
Gongbujiangda	Nyang river	2006~2009, wet season
Yangbajing	Lhasa river	2006~2015, wet season
Pangduo	Lhasa river	2001~2015, wet season
Tangjia	Lhasa river	2001~2015, wet season

163 Grab samples of precipitation and stream water were collected in 2005 at four stations
164 along the mainstream of YTR, i.e., Lazi, Nugesha, Yangcun, and Nuxia, from upstream to
165 downstream, for isotope analysis (Table 2, Liu et al., 2007). The outputs of Scripps Global
166 Spectral Model with isotope incorporated (isoGSM, Yoshimura et al., 2008) with 1.875°
167 resolution were extracted to represent the spatiotemporal variation of precipitation isotope in
168 the YTR basin. According to our previous assessment based on the measurement precipitation

169 isotope data, the isoGSM captured the seasonality of precipitation isotope well, but had
 170 systematic overestimation biases in the YTR basin, which were highly correlated to the altitude
 171 (Nan et al., 2021a). The corrected isoGSM in the YTR basin produced by Nan et al. (2022) was
 172 adopted in this study.

173 **Table 2.** Summary of measurement isotope data in the YTR basin during 2005

Station	Period	Precipitation			Stream		
		Number of samples	$\overline{\delta^{18}\text{O}}$ (‰)	SD (‰)	Number of samples	$\overline{\delta^{18}\text{O}}$ (‰)	SD (‰)
Nuxia	14 Mar. – 23 Oct.	86	-10.33	7.18	34	-15.74	1.60
Yangcun	17 Mar. – 5 Oct.	59	-13.17	7.10	30	-16.57	1.69
Nugesha	14 May. – 22 Oct.	45	-14.29	7.99	25	-17.84	0.99
Lazi	6 Jun. – 22 Sep.	42	-17.41	5.75	22	-16.52	1.43

174 **2.3 The tracer-aided hydrological model**

175 A distributed tracer-aided hydrological model, Tsinghua Representative Elementary
 176 Watershed-Tracer-aided version (THREW-T) model, developed by Tian et al. (2006) and Nan
 177 et al. (2021b), was adopted to simulate the hydrological and isotopic processes in the YTR basin.
 178 The model uses the representative elementary watershed (REW) method for spatial
 179 discretization of basins, dividing the whole catchment into REWs based on DEM data. Each
 180 REW is further divided into two vertically distributed layers (i.e., surface and subsurface layers),
 181 including eight subzones (i.e., surface layer: vegetation zone, bare zone, main channel reach
 182 zone, sub stream network zone, snow-covered zone, and glacier-covered zone; subsurface layer:
 183 unsaturated zone and saturated zone) (Reggiani et al., 1999; Tian et al., 2006). This study
 184 divided the YTR basin into 297 REWs, with an average area of 694 km², ranging from 162 to
 185 2753 km². More model details are provided in Tian et al. (2006).

186 A cryospheric module representing the evolutions of snowpack and glacier was
 187 incorporated into the model for application in cold regions. The total precipitation was
 188 partitioned into liquid and solid precipitation according to a temperature threshold, which was
 189 set as 0°C. The degree-day factor method was used to calculate the meltwater. The snow water
 190 equivalent of each REW was updated based on the snowfall (i.e., the solid precipitation) and
 191 the snowmelt, and the snow cover area was then determined by the snow cover depletion curve
 192 (Fassnacht et al., 2016). To simulate the evolution of glaciers, each REW is further divided into

193 several elevation bands to represent the change in temperature and precipitation along the
194 altitudinal profile. The glacier within the intersection of each REW and elevation band is
195 regarded as the representative unit for glacier simulation, similar to the discretization strategy
196 adopted by Luo et al. (2013). For each glacier simulation unit, the model simulates the processes
197 including the accumulation and melt of snow over glacier, the turnover of snow to ice, and the
198 ice melt. More details and equations of the cryospheric module are provided in Nan et al. (2021b)
199 and Cui et al. (2023).

200 The tracer module was incorporated into the model to simulate the isotope composition of
201 multiple water bodies. The Rayleigh equation was adopted to simulate the isotope fractionation
202 during water evaporation and snowmelt processes (He et al., 2019; Hindshaw et al., 2011). The
203 isotope composition of glacier meltwater was assumed to be constantly more depleted than the
204 local precipitation isotope and was estimated by an offset parameter (Nan et al., 2022). The
205 isotope compositions in each simulation unit were calculated based on the complete mixing
206 assumption. The isotope composition of snowpack and snowmelt was updated based on the
207 water and isotope mass balance of the snowpack, similarly with other water storages. Forced
208 by the precipitation isotope composition, the model can simulate the isotope composition of all
209 water bodies, including stream water, soil water, groundwater, and snowpack. More details and
210 calculation equations of the tracer module are provided in Nan et al. (2021b).

211 The THREW-T model quantified the contributions of multiple runoff components based
212 on the flow-pathway definition as reviewed by He et al. (2021a). The runoff was firstly divided
213 into surface runoff and subsurface runoff (baseflow) based on the runoff generation pathway.
214 The surface runoff was then further divided into three components induced by different water
215 sources (rainfall, snowmelt, and glacier melt). As a result, the total runoff was divided into four
216 components: subsurface runoff, rainfall overland runoff, snowmelt overland runoff, and glacier
217 melt overland runoff.

218 **2.4 Model calibration and evaluation**

219 The model was run for 25 years starting from 1991 to 2015, and was calibrated toward
220 four objectives: the discharge at Nuxia station from 2001 to 2015, the snow cover area (SCA)
221 from 2001 to 2015, the average glacier mass balance (GMB) from 2001 to 2010 in the whole

222 YTR basin, and the stream water isotope at the four stations in 2005. The Nash-Sutcliffe
223 efficiency (NSE) was set as the evaluation metric for objectives with strong seasonality
224 (discharge and isotope), and the root mean square error (RMSE) was set as the evaluation metric
225 for objectives with essentially fluctuations (SCA and GMB) (Schaefli and Gupta, 2007). The
226 optimization objective function of calibration procedure was calculated by combining the
227 function of each objective with equal weights.

228 An automatic algorithm, the Python Surrogate Optimization Toolbox (pySOT, Eriksson et
229 al., 2019) were adopted for model calibration. The pySOT algorithm uses radial basis functions
230 (RBFs) as surrogate models to approximate the simulations, reducing the time for each model
231 run. The symmetric Latin hypercube design (SLHD) method was used to generate parameter
232 values, allowing an arbitrary number of design points. In each optimization run, the procedure
233 stopped when a maximum number of allowed function evaluations was reached, which was set
234 as 3000. In this study, the pySOT algorithm was repeated for 100 times, and a final parameter
235 set was selected from the calibrated parameter sets manually based on the overall performance
236 on multiple objectives. The physical basis, reference ranges and calibrated values of the
237 calibrated parameters in the THREW-T model are shown in Table 3.

238 Apart from the calibration functions, the model performances were additionally evaluated
239 by four statistical metrics: logarithmic NSE (lnNSE), RMSE-observations standard deviation
240 ratio (RSR), Percent bias (PBIAS) and correlation coefficient (CC). The discharge simulation
241 was evaluated by lnNSE to examine the simulation of baseflow process. Our previous studies
242 indicated that the discharge simulation performance during validation was highly correlated
243 with that of calibration period, partly due to the strong linearity of precipitation-discharge
244 relation in such a large basin, but large uncertainties existed in the discharge simulation at
245 internal stations even when the discharge at outlet station was simulated well (Nan et al., 2021b,
246 2022). Consequently, we not only conducted temporal validation based on the discharge data
247 at Nuxia station during 1991~2000, but also collected additional discharge data at eight internal
248 stations to assess the spatial consistency of model performance. The RMSE and CC of the
249 cumulative glacier mass balance since the beginning of simulation period were also calculated
250 to assess the glacier simulation, considering the temporal interpolation adopted by Hugonnet et
251 al. (2021) which led to uncertainty in the year scale data.

$$252 \quad \text{NSE} = 1 - \frac{\sum(X_o - X_s)^2}{\sum(X_o - \bar{X}_o)^2} \quad (1)$$

$$253 \quad \text{lnNSE} = 1 - \frac{\sum(\ln(X_o) - \ln(X_s))^2}{\sum(\ln(X_o) - \ln(\bar{X}_o))^2} \quad (2)$$

$$254 \quad \text{RMSE} = \sqrt{\frac{\sum(X_o - X_s)^2}{n}} \quad (3)$$

$$255 \quad \text{RSR} = \frac{\text{RMSE}}{\text{STD}_{\text{obs}}} = \frac{\sqrt{\sum(X_o - X_s)^2}}{\sqrt{\sum(X_o - \bar{X}_o)^2}} \quad (4)$$

$$256 \quad \text{PBIAS} = \frac{\sum(X_o - X_s) * 100}{\sum X_o} \quad (5)$$

$$257 \quad \text{CC} = \frac{\sum[(X_s - \bar{X}_s)(X_o - \bar{X}_o)]}{\sqrt{\sum[(X_s - \bar{X}_s)^2(X_o - \bar{X}_o)^2]}} \quad (6)$$

258 where, X_s , X_o , \bar{X}_s and \bar{X}_o are the simulated, observed, mean of simulated and mean of
 259 observed hydrological variables, respectively, and n is the number of data.

260 **Table 3.** Physical descriptions, reference ranges and calibrated values of the calibrated
 261 parameters in the THREW-T model

Symbol	Unit	Description	Reference range	Calibrated value
WM	cm	Tension water storage capacity used to calculate the saturation area	0~10	2.92
B	-	Shape coefficient used to calculate the saturation area	0~1	0.04
KKA	-	Exponential coefficient to calculate the subsurface runoff outflow rate	0~6	5.92
KKD	-	Linear coefficient to calculate the subsurface runoff outflow rate	0~0.5	0.21
DDF _s	Mm/°C/d	Degree day factor for snowmelt	0~10	2.60
DDF _G	Mm/°C/d	Degree day factor for glacier melt	0~10	1.51
T ₀	°C	Temperature threshold above which snow and glaciers melting occurs	-5 ~ 5	-4.28
C ₁	-	Coefficient to calculate concentration process using the Muskingum method	0~1	0.04
C ₂	-	Coefficient to calculate concentration process using the Muskingum method	0~1	0.80

262 2.5 Perturbed climatic scenarios design

263 Daily temperature and precipitation data extracted from the CMFD dataset were set as the
 264 reference climate inputs. Linearly perturbed temperature and precipitation time series were
 265 adopted to represent the potential climate change ranges. Perturbed temperature input data was
 266 generated by adding one-degree increments to the reference daily temperature. The maximum

267 temperature increase was set as 5 °C, because the temperature in the YTR basin is projected to
 268 increase at 1°C/20 yrs, and will increase by about 5 °C until the end of this decade (Cui et al.,
 269 2023). The influence of changing temperature on the potential evapotranspiration was estimated
 270 by the regression between the two factors (Eq. 7) which was developed by Van Pelt et al. (2009)
 271 and widely adopted in the projection of potential evapotranspiration (e.g., Xu et al., 2019; Cui
 272 et al., 2023).

$$273 \quad E_p = [1 - \alpha_0(T - \bar{T}_0)] \cdot \bar{E}_{p0} \quad (7)$$

274 where, \bar{T}_0 and \bar{E}_{p0} are the mean daily temperature and potential evapotranspiration in each
 275 REW during the simulation period, respectively. T is the daily temperature generated by the
 276 perturbation method. α_0 is determined by regressing the input daily potential
 277 evapotranspiration and temperature in each REW.

278 Perturbed precipitation input data was generated by multiplying the reference daily
 279 precipitation data from 80% to 120% with an increment of 10%, similar to Su et al. (2023)
 280 which analyzed the runoff change of three basins on the TP under hypothesized climate change
 281 scenarios. Simulation during 2001~2015 was set as the reference scenario, because the data of
 282 most objectives/stations were available during this period. In total, one reference simulation,
 283 five simulations of perturbed temperature and four simulations of perturbed precipitation were
 284 conducted. To focus on the influence of climate perturbations on the hydrological processes,
 285 the changes of underlying conditions such as soil and vegetation were not considered. In each
 286 scenario, the standard deviations (STD) of the simulated annual hydrological variables were
 287 calculated to represent the uncertainties introduced by natural climate variability. The t-Test
 288 analysis of paired two samples was conducted for the annual hydrological variables produced
 289 by reference scenario and each climate perturbation scenarios, to analyze the statistical
 290 significance of the changes. Apart from the basic hydrological variables, the concentration ratio
 291 (CR) and concentration period (CP) (Jiang et al., 2022a) were calculated by Eqs. 8~10 to
 292 characterize the runoff seasonality.

$$293 \quad CR = \sqrt{R_x^2 + R_y^2} / \sum_{i=1}^{12} R_i \quad (8)$$

$$294 \quad CP = \arctan (R_x/R_y) \quad (9)$$

$$295 \quad R_x = \sum_{i=1}^{12} R_i \times \sin (\theta_i); R_y = \sum_{i=1}^{12} R_i \times \cos (\theta_i) \quad (10)$$

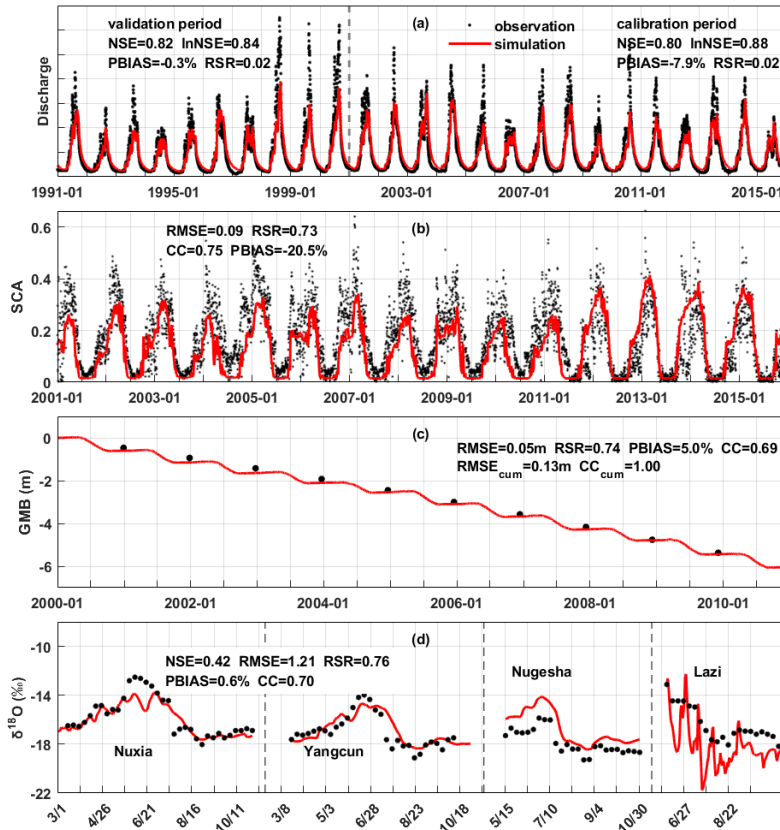
296 where, R_i is the runoff in the i th month, R_x and R_y are the resulting vectors in the direction of x
297 and y , respectively. $\theta=360^\circ/12\times i=30^\circ\times i$ ($i=1,2,\dots,12$).

298 **3. Results**

299 **3.1 Model performance evaluation**

300 Figure 2 shows the model performances on the four calibration objectives. The discharge
301 was simulated well regarding both high flow and baseflow processes, as indicated by the high
302 NSE (0.82) and lnNSE (0.84). The occurring times of peak flow were captured by the model,
303 showing the consistency in the temporal dynamics of simulated and observed streamflow, but
304 the simulated magnitudes of peak flow were slightly lower than the observation (Figure 2a),
305 partly due to the poor abilities of precipitation products on accurately capturing the high
306 precipitation in high elevation elevations and the amount of specific precipitation extreme
307 events (Li et al., 2021; Jiang et al., 2022b; Xu et al., 2017). The performance of discharge
308 simulation during validation period was similar with that of calibration period, with NSE and
309 lnNSE of 0.80 and 0.88 respectively, as shown in Figure 2a. Nonetheless, the simulated annual
310 runoff (302 mm/yr) was very close to the observation (303 mm/yr), indicating that the amount
311 of total runoff was reproduced well. The simulated variation of SCA was smoother than the
312 observation, but the seasonality was captured well, i.e., decreasing sharply in May and
313 remaining extremely low from July to September (Figure 2b). The low RMSE (<0.1) suggested
314 that the model performed well on simulating the snow processes. The model successfully
315 simulated the declining glacier (Figure 2c), with an extremely high CC for the cumulative
316 glacier mass balance (~ 1). The model estimated the annual GMB in the YTR basin as -0.545
317 m/yr, very close to the value extracted from the dataset of Hugonnet et al. (2021) (-0.554 m/yr).
318 The calibrated melting temperature threshold was rather low (-4.28°C), which was partly due
319 to the fact that melting processes were simulated at the daily step. The model simulated the
320 variation of stream isotope well, indicated by the high NSE, CC and low PBIAS, which
321 provided confidence in the partitioning among different runoff components (Nan et al., 2021a;
322 He et al., 2019). The seasonality of the isotope was adequately captured: getting enriched in
323 May, reaching maximum in June, and getting depleted in late June/early July (Figure 2d). The
324 fact that the model simultaneously satisfied four calibration objectives ensured the proper

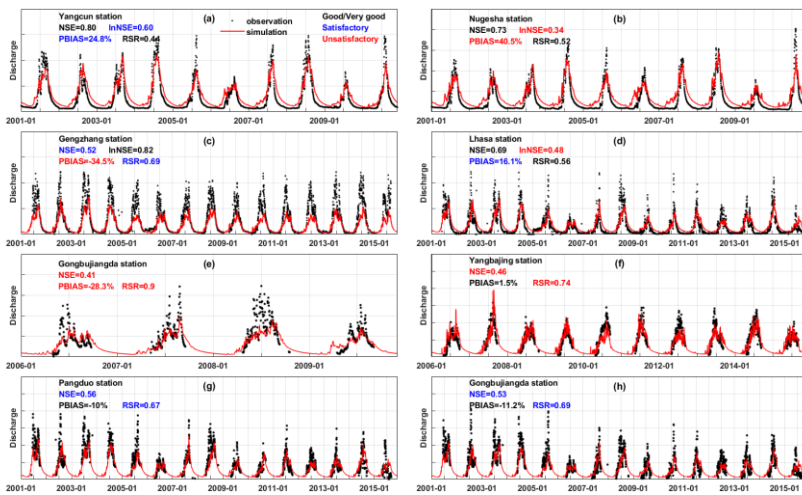
325 representation of the hydrological and cryospheric processes, and provided a reasonable
 326 baseline for the sensitivity analysis.



327
 328 **Figure 2.** The model performances on the calibration objectives. (a) the streamflow discharge
 329 at Nuxia station, (b) the snow cover area ratio in the YTR basin, (c) the average glacier mass
 330 balance in the YTR basin, and (d) the stream water isotope at four stations in 2005.

331 Figure 3 shows the streamflow simulation at eight internal stations. The performance
 332 ratings were evaluated based on four metrics following the guideline by Moriasi et al. (2007).
 333 At the two stations located along the mainstream (Yangcun and Nugesha), the high flow
 334 processes were simulated well as indicated by the high NSE, but the baseflows were
 335 overestimated (Figure 3a and b). In contrast, the high flow processes were underestimated at
 336 Gengzhang station, but the baseflows were reproduced well (Figure 3c). The model produced
 337 fair performance on both high flow and baseflow simulation at Lhasa station, showing moderate

338 NSE and lnNSE (Figure 3d). For the four stations where only the data during the wet season
 339 were available, the PBIASs were at good levels (within $\pm 15\%$) except for Gongbujiangda
 340 station (Figure 3e-h). Overall, the streamflow simulations at internal stations were not as good
 341 as the calibrated outlet station, but were at acceptable levels, as indicated by at least one
 342 satisfactory metric except for Gongbujiangda station. The high flow processes and runoff
 343 amount were reproduced relatively well, as indicated by the generally satisfactory NSE and
 344 PBIAS. But the small time-scale fluctuations and extremes were mostly not captured well,
 345 because the model was not evaluated toward metrics related to hydrological signatures
 346 (McMillan et al., 2017; Majone et al., 2022; Fenicia et al., 2018). Nonetheless, the validation
 347 based on the internal stations gave confidence in the spatial pattern of the hydrological
 348 processes and their sensitivities to the perturbed climate.

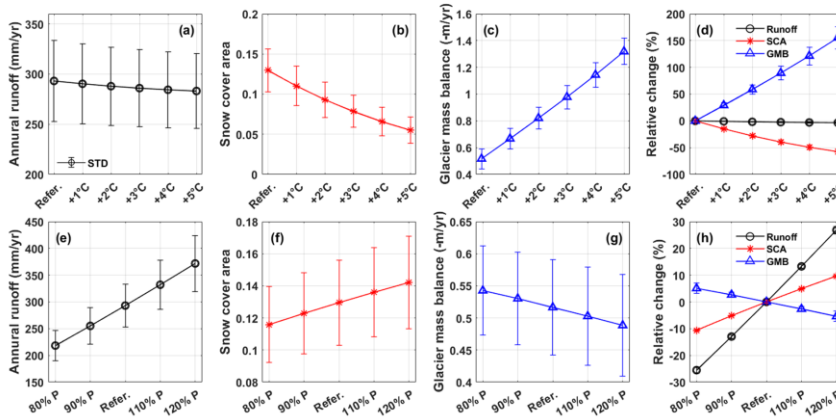


349
 350 **Figure 3.** The model performances on the streamflow simulation at the internal stations.

351 **3.2 Sensitivities of hydrological variables to perturbed temperature and precipitation**

352 The sensitivities of annual runoff, snow cover area, and glacier mass balance to perturbed
 353 temperature and precipitation are shown in Figure 4. The relationships between hydrological
 354 variables and precipitation/temperature showed strong linearity, which was similar with Su
 355 et al. (2023) analyzing the hydrological sensitivities in three other large basins on the TP ($\sim 10^5$
 356 km^2), but was different from He et al. (2021b) which conducted a similar analysis in a small
 357 boreal forest basin in Canada (603 km^2). The annual runoff kept decreasing significantly with

358 the increasing temperature at the rate of $-2 \text{ mm}/^\circ\text{C}$ due to the increasing evaporation (Figure
 359 4a). The decreasing rate got small when the temperature increase was higher than 3°C , partly
 360 because the controlling factor of evaporation changed from energy limitation to water limitation
 361 (Wang et al., 2022). The runoff change in response to increasing temperature was rather small
 362 compared to the intra-annual runoff variability. The snow cover area ratio significantly reduced
 363 with the increasing temperature at the rate of $-1.5\%/^\circ\text{C}$ because of the decreasing snowfall and
 364 increasing snowmelt, and would be smaller than half of the reference scenario for 5°C of
 365 warming (Figure 4b). The glacier mass balance significantly got more negative with the
 366 increasing temperature because of the reducing accumulation and increasing meltwater, at the
 367 rate of $-0.16 \text{ m}/^\circ\text{C}$ (Figure 4c). Among the three variables, the glacier mass balance was the
 368 most sensitive to the warming climate, the relative change of which could be 150% for 5°C of
 369 warming (Figure 4d). The changes of runoff, snow cover area and glacier mass balance in
 370 response to increasing temperature were all statistically significant at 0.01 significance level.



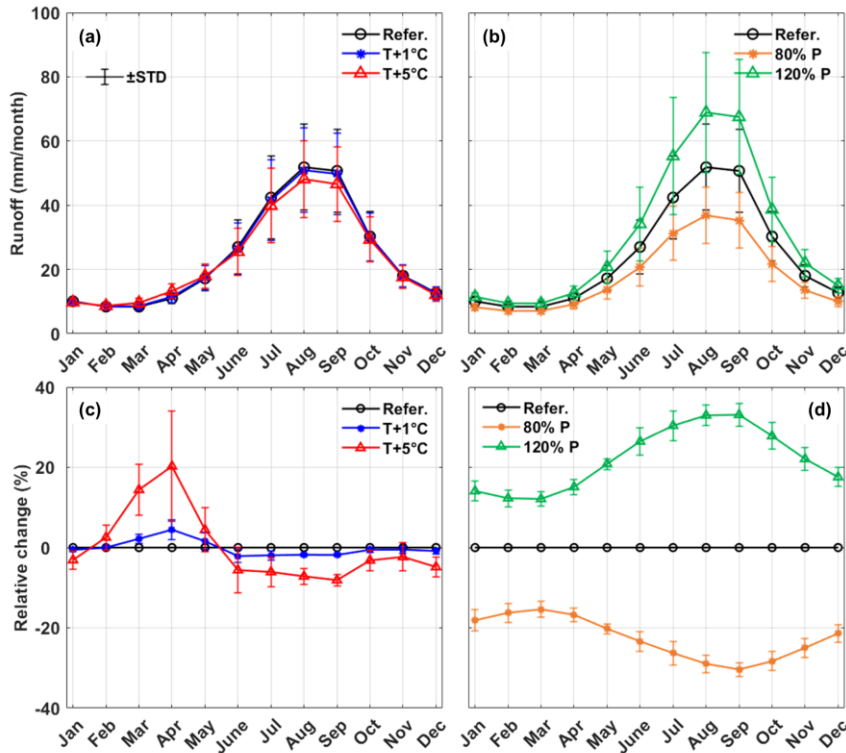
371
 372 **Figure 4.** The sensitivities of annual runoff, snow cover area, and glacier mass balance to the
 373 perturbed temperature (a-d) and precipitation (e-g). Subplots (d) and (h) are the relative changes
 374 of runoff, SCA and GMB compared to the reference scenario.

375 The hydrological sensitivities to perturbed precipitation were opposite to that of
 376 temperature. The annual runoff increased at the rate of $38.4 \text{ mm}/10\%$ with the increasing
 377 precipitation (Figure 4e). The relative change in runoff was larger than precipitation (Figure
 378 4h), indicating an increasing runoff coefficient with increasing precipitation. This also indicated

379 a small relative change in evaporation in response to precipitation perturbation, again
380 suggesting that the energy limitation played more important role than water limitation on
381 evaporation in the reference scenario. With the increasing precipitation, the snow cover area
382 increased at 0.7%/10%, and the glacier mass balance got more positive at 0.014m/10% because
383 of the larger amount of snowfall and snow/ice accumulation (Figure 4f and 4g). Among the
384 three variables, the runoff had the highest sensitivity to perturbed precipitation, with a relative
385 change rate of 13%/10% (Figure 4h), while the changes of snow cover area and glacier mass
386 balance were within the range of $\pm 10\%$ when precipitation changed by 20%. The changes of
387 runoff, snow cover area and glacier mass balance in response to perturbed precipitation were
388 all statistically significant at 0.01 significance level.

389 **3.3 Sensitivities of runoff variation to perturbed temperature and precipitation**

390 The sensitivities of inter- and intra-annual runoff variation to perturbed temperature and
391 precipitation are shown in Figure 5. The average monthly runoff were calculated based on the
392 simulated hydrographs during the entire simulation period, and the inter-annual runoff variation
393 was represented by the STD. The change of inter-annual runoff variation was consistent with
394 that of total runoff. The inter-annual runoff variations were also lower in the scenarios with less
395 runoff (increasing temperature or decreasing precipitation), showing the narrower ranges of the
396 error bars in Figure 5a-b, and vice versa. Despite the decreasing runoff caused by increasing
397 temperature, the average runoff for 5°C of warming was still much higher than the lower error
398 bar of the reference scenario (Figure 5a), suggesting that the runoff change tendency caused by
399 the increasing temperature was relatively small compared to the inherent runoff variability. On
400 the contrary, when precipitation increased by 20%, the average annual runoff was higher than
401 the runoff in wet years of reference scenario (Figure 5b), indicating that the trend of
402 precipitation change had a larger influence on the runoff than the inter-annual variation of
403 precipitation.



404
 405 **Figure 5.** Sensitivities of intra- and inter-annual streamflow variability to the perturbed
 406 temperature and precipitation. (a) and (b) monthly runoff, (c) and (d) relative change of monthly
 407 runoff.

408 The sensitivities of monthly runoff were different among months. Although increasing
 409 temperature led to a decrease in the total runoff, it caused an increasing spring runoff. The
 410 monthly runoff in April increased most significantly, which increased 20% for 5°C of warming
 411 (Figure 5e). This could be attributed to the increasing snowmelt, because the SCA decreased
 412 significantly during the same period (Figure 2b). The monthly runoff in all twelve months
 413 changed accordingly to perturbed precipitation, but the change during wet seasons (August to
 414 October) was the most significant (Figure 5f). The different monthly runoff sensitivities in
 415 response to perturbed temperature and precipitation indicated that temperature changes
 416 influenced more on baseflow, while precipitation changes had higher impact on high flow
 417 processes. As a result, increasing temperature caused a more even distribution of monthly

418 runoff, while increasing precipitation had the opposite effect. The CR decreased from $0.432 \pm$
 419 0.044 to 0.402 ± 0.046 for the warming of 5°C , indicating a more even seasonal runoff
 420 distribution caused by increasing temperature. The CP decreased by around two days, indicating
 421 that climate warming would result in advance of maximum runoff. The STD of CP slightly
 422 increased from 7.09 days at the reference scenario to 7.45 days for the warming of 5°C . On the
 423 contrary, the CR changed from 0.398 ± 0.039 to 0.465 ± 0.045 when precipitation increased from
 424 80% to 120% of the reference, indicating that increasing precipitation made the distribution of
 425 runoff more concentrated. The CP advanced by 2.2 days in response to a 20% decreasing
 426 precipitation, but only recessed by 0.3 days in response to an increasing precipitation with the
 427 same magnitude. Similar with the response to warming temperature, the STD of CP also slightly
 428 increased in response to increasing precipitation. The change of CR was significant at
 429 significance level of 0.01 in all scenarios, but the change of CP was insignificant in some
 430 scenarios, including T $+1^\circ\text{C}$, 110% P and 120% P, with p value of 0.014, 0.02 and 0.12,
 431 respectively.

432 **Table 4.** The concentration ratio (CR) and concentration period (CP) of runoff in different
 433 scenarios with perturbed temperature and precipitation

		CR		CP (days)	
		Average	STD	Average	STD
Reference scenario		0.432	0.044	244.4	7.09
T scenario	+1°C	0.425	0.044	244.1	7.12
	+2°C	0.419	0.045	243.8	7.18
	+3°C	0.413	0.045	243.3	7.26
	+4°C	0.408	0.046	242.8	7.36
	+5°C	0.402	0.046	242.3	7.45
P scenario	80%	0.398	0.039	242.2	6.86
	90%	0.415	0.042	243.6	7.01
	110%	0.449	0.045	244.7	7.13
	120%	0.465	0.045	244.7	7.14

434 3.4 Sensitivities of runoff components to perturbed temperature and precipitation

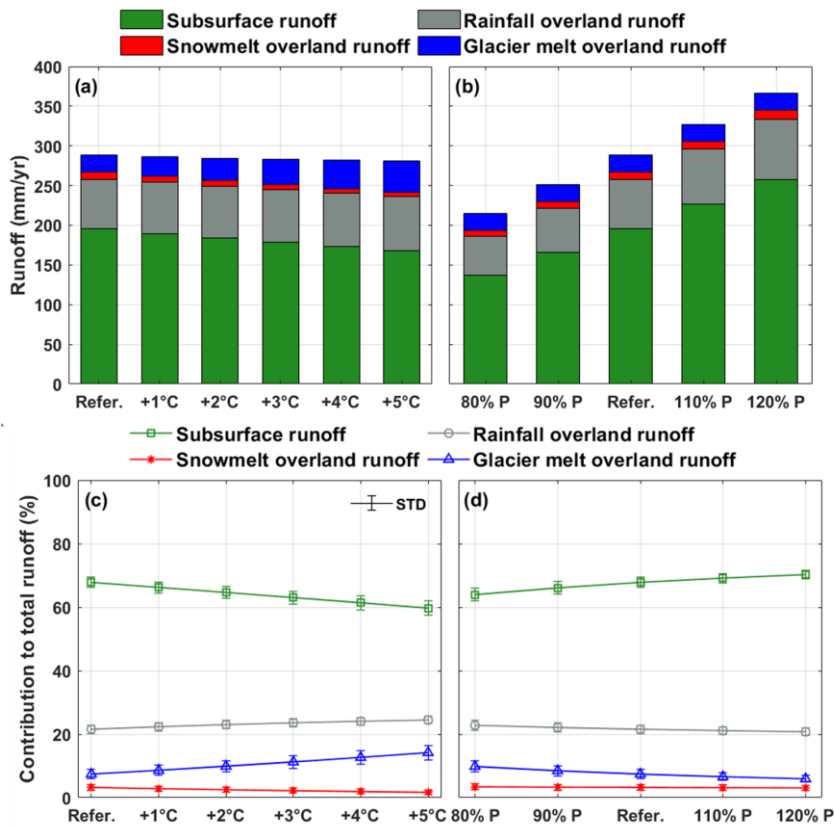
435 The contributions of runoff components in the YTR basin under scenarios with different
 436 temperature and precipitation are shown in Figure 6. In the reference scenario, the subsurface
 437 runoff was the dominant component, contributing $67.8 \pm 1.7\%$ to the total runoff. Among the
 438 three surface runoff components, rainfall was the dominant water source contributing $21.6 \pm$

设置了格式: 复杂文种字体: Times New Roman

设置了格式: 复杂文种字体: Times New Roman

439 1.3% to the total runoff. Glacier melt overland runoff had considerable contribution to the
 440 runoff which contributed $7.4 \pm 1.4\%$ to the total runoff, while the contribution of snowmelt
 441 overland runoff was only $3.2 \pm 0.9\%$. The annual subsurface runoff was 195.8 ± 31.0 mm/yr (39.2
 442 ± 6.2 km³/yr), close to the amount (30 km³/yr) estimated by Yao et al. (2021) with the
 443 groundwater model MODFLOW. It should be noted that in our model all the glacier meltwater
 444 was assumed to generate surface runoff directly because of the impermeable glacier surface,
 445 while the snowmelt was assumed to be partitioned into two components (infiltration and surface
 446 runoff) (Nan et al., 2021b, 2023; Schaepli et al., 2005).

设置了格式: 复杂文种字体: Times New Roman
 设置了格式: 复杂文种字体: Times New Roman
 设置了格式: 复杂文种字体: Times New Roman
 设置了格式: 复杂文种字体: Times New Roman



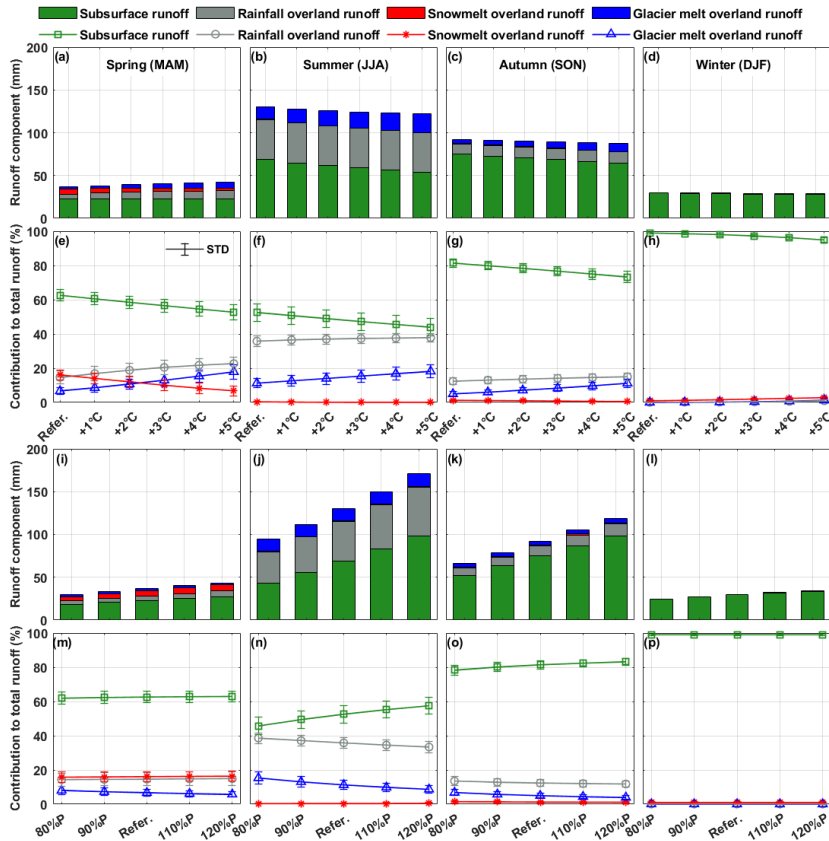
447
 448 **Figure 6.** Sensitivities of the runoff components to perturbed temperature and precipitation.
 449 (a) and (b) amounts of runoff components, (c) and (d) contributions of runoff components to
 450 the total runoff.

451 With the increasing temperature, the amount and proportion of subsurface runoff decreased

452 at $-5.6\text{mm}/^{\circ}\text{C}$ and $-1.6\%/^{\circ}\text{C}$, because climate warming increased evaporation and consequently
453 reduced the subsurface water storage and outflow. The rainfall and snowmelt overland runoff
454 increased at $1.3\text{mm}/^{\circ}\text{C}$ ($0.6\%/^{\circ}\text{C}$) and decreased at $-0.9\text{mm}/^{\circ}\text{C}$ ($-0.3\%/^{\circ}\text{C}$), respectively,
455 because more rainfall was partitioned from total precipitation due to higher temperature. The
456 glacier melt overland runoff increased significantly at $3.7\text{mm}/^{\circ}\text{C}$ ($1.4\%/^{\circ}\text{C}$) with the increasing
457 temperature, and the contribution to total runoff could be around 15% for 5°C of warming. The
458 amount of all four runoff components increased with the increasing precipitation (Figure 6b),
459 with rates of $30.1\text{mm}/10\%$, $6.8\text{mm}/10\%$, $1.0\text{mm}/10\%$ and $0.1\text{mm}/10\%$ for subsurface, rainfall
460 overland, snowmelt overland and glacier melt overland runoff, respectively. However, only the
461 proportion of subsurface runoff increased at $1.6\%/10\%$ with the increasing precipitation, while
462 the proportions of three other components all decreased, with rates of $-0.5\%/10\%$, $-0.1\%/10\%$
463 and $-1.0\%/10\%$ for rainfall overland, snowmelt overland and glacier melt overland runoff,
464 respectively (Figure 6d), because there was a much higher increase in the total runoff. Overall,
465 the contributions of runoff components were more sensitive to temperature perturbation than
466 precipitation perturbation.

467 Figure 7 and Tables S1-S4 show the runoff components in different seasons and their
468 sensitivities to perturbed climate. The subsurface runoff was the dominant component in all
469 four seasons in the reference scenario, with contribution ranging from 53% in summer to 99%
470 in winter. The contribution of snowmelt overland runoff was extremely low in the seasons
471 except for spring because of the small SCA in summer and autumn and the low temperature in
472 winter. The contribution of snowmelt overland runoff in spring was close to that of rainfall
473 overland runoff (Figure 7e-h). The contribution of glacier melt overland runoff was around half
474 that of rainfall overland runoff in all four seasons. With climate warming, the contribution of
475 subsurface runoff decreased in all four seasons, while the contributions of rainfall and glacier
476 melt overland runoff increased. The significantly increasing glacier melt and rainfall led to an
477 increase in the total runoff in spring (Figure 7a). The contribution of snowmelt overland runoff
478 decreased in three seasons except for winter, during which its contribution slightly increased,
479 and got around 3% for 5°C of warming (Figure 7h). With increasing precipitation, the amounts
480 of four components increased in all seasons (Figure 7i-l), but the contributions of components
481 remained nearly unchanged in spring, autumn and winter (Figure 7m, o-p). The contributions

482 of runoff components were sensitive to perturbed precipitation only in summer, during which
 483 subsurface runoff contributed more to the runoff with increasing precipitation, while the
 484 contributions of rainfall and glacier melt overland runoff decreased significantly (Figure 7n).



485 **Figure 7.** Sensitivities of the seasonal runoff components to perturbed temperature and
 486 precipitation. (a)-(d) sensitivities of amounts of runoff components to perturbed temperature,
 487 (e)-(h) sensitivities of contributions of runoff components to perturbed temperature, (i)-(l)
 488 sensitivities of amounts of runoff components to perturbed precipitation, (m)-(p) sensitivities
 489 of contributions of runoff components to perturbed precipitation.

491 **3.5 Spatial pattern of local hydrological sensitivities**

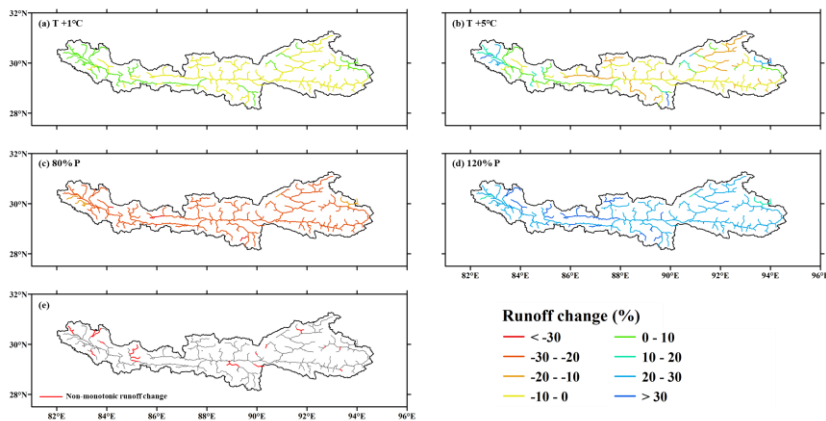
492 Considering that the YTR basin is a large basin with drainage area of 2×10^5 km², the spatial
 493 pattern of the local hydrological sensitivity was further analyzed with the assistance of the

494 spatially distributed model structure. The runoff change at REW scale in four typical scenarios
495 (i.e., 1°C of warming, 5°C of warming, precipitation changing to 80% and 120%) are shown in
496 Figure 8. All REWs have the same runoff trend with the precipitation perturbation (Figure 8c
497 and 8d). The runoff increasing ranged from 12.2% to 40.4% when precipitation increased by
498 20%. In most REWs, the runoff changed at larger rates than precipitation, with few exceptions
499 located in the tributaries of Nyang River, Lhasa River and the source region of mainstream,
500 showing shallow red/blue colors in Figure 8c and 8d. On the contrary, the REW scale runoff
501 changes in response to increasing temperature had strong spatial variability (Figure 8a and 8b).
502 Although the runoff at the basin outlet decreased with climate warming, the REW scale runoff
503 increased in about half of REWs. For 5°C of warming, the REW scale runoff changes ranged
504 from -18.6% to 54.3%. Most REWs with increasing runoff were located upstream of the
505 mainstream, the Nianchu River, the Nyang River, and the tributary of Lhasa River (Figure 8b).

506 The statistical significance of runoff change in response to climate perturbation was
507 analyzed. The runoff change in response to perturbed precipitation was significant in all the
508 REWs, but things were different for warming temperature scenarios. The number of REWs
509 with insignificant change trend decreased with the temperature warming level. In specify, the
510 runoff change was insignificant (at significance level of 0.01) in 26% and 15% area of the whole
511 basin, for the warming of 1°C and 5°C, respectively (Figure S1). The statistical significance in
512 response to warming temperature was related to the runoff change magnitude and drainage area
513 (Figure S2). Consequently, although the runoff change at basin outlet was rather small
514 (decreasing by 0.9% and 3.4% for the warming of 1°C and 5°C, respectively), it was still
515 statistically significant.

516 The runoff in some REWs changed non-monotonically with increasing temperature, i.e.,
517 the runoff change trend was reversed in different temperature intervals. Most of such non-
518 monotonic REWs were located in the upstream region of the mainstream, with some others
519 located in the major tributaries Nyang River, Lhasa River and Nianchu River (Figure 8e). In
520 about 75% of non-monotonic REWs, the runoff first decreased for 1°C of warming, and then
521 changed to an increasing trend at higher warming levels, and the reserved trends occurred in
522 the other 25% of REWs. The threshold temperature of trend turning differed among non-
523 monotonic REWs, which was 3°C in about half of the REWs. The runoff change rates in

524 response to increasing temperature were generally low in non-monotonic REWs, most within
525 the range of $\pm 1\%/^{\circ}\text{C}$.



526
527 **Figure 8.** The change of REW scale runoff in response to perturbed temperature and
528 precipitation. (a) and (b) runoff change in response to temperature perturbation, (c) and (d)
529 runoff change in response to precipitation perturbation, (e) the locations of REWs showing non-
530 monotonic runoff change in response to increasing temperature.

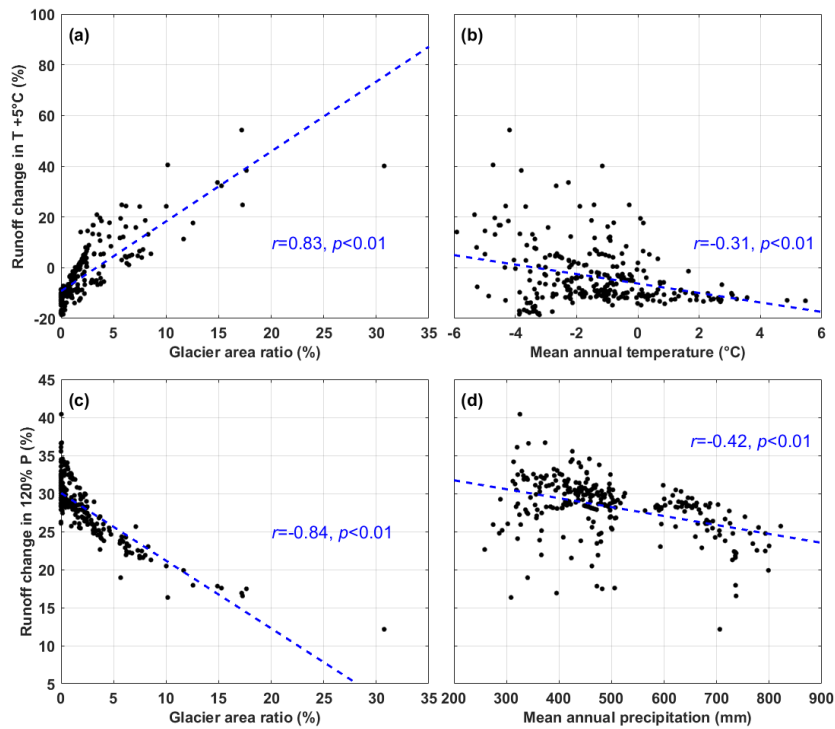
531 4. Discussions

532 4.1 The influence factors of local hydrological sensitivities: the role of glaciers

533 Our results show the strong spatial variability of the REW scale hydrological sensitivities
534 to perturbed climate. Consequently, the influence factors of the local sensitivities are analyzed
535 in this section. The basic characteristics, including mean annual temperature (MAT), mean
536 annual precipitation (MAP), average elevation (ELE), drainage area (DRA), and glacier area
537 ratio (GAR) were calculated for each REW as the potential factors. It should be noted that,
538 considering the runoff concentration processes between the upstream and downstream REWs,
539 the above characteristics were not calculated solely within each REW, but for the total drainage
540 area controlled by each REW. The correlations between the runoff change for
541 temperature/precipitation increasing by $5^{\circ}\text{C}/20\%$ and the potential influence factors were
542 analyzed. The relations with the two factors with the highest coefficients are shown in Figure
543 9. Detailed data and relations with lower coefficients are shown in Table S5 and Figure S3.

544 The GAR was the most correlated factor for the hydrological sensitivities to the

545 perturbation of both temperature and precipitation, with coefficients higher than 0.8 (Figure 9a
546 and 9c). The runoff change for 5°C of warming increased with the increasing GAR (Figure 9a),
547 because of the balance between the decreasing runoff caused by evaporation and the increasing
548 runoff contributed by glacier melt. In REWs where the GAR was higher than a threshold, the
549 increasing glacier melt could offset the increasing evaporation, and the runoff increased with
550 climate warming. The threshold GAR was different among REWs, ranging from 1~5%. For the
551 REWs with GAR larger than 10%, the runoff increase for 5°C of warming could be higher than
552 20%. The hydrological sensitivity to increasing temperature also had a weak but significant
553 negative correlation ($r=-0.31$, $p<0.01$) with the MAT of the REW (Figure 9b), which could be
554 partly attributed to the interrelation between GAR and MAT, i.e., the GAR tended to be lower
555 in warmer regions, and the runoff consequently decreased in response to increasing temperature.
556 A lower bound of runoff change could be observed in Figure 9b for the REWs with relatively
557 high MAT, again indicating the different limitation factors of evaporation, i.e., in relatively
558 warm regions, the evaporation was limited by the water condition, so increasing temperature
559 did not cause more evaporation (Wang et al., 2022).



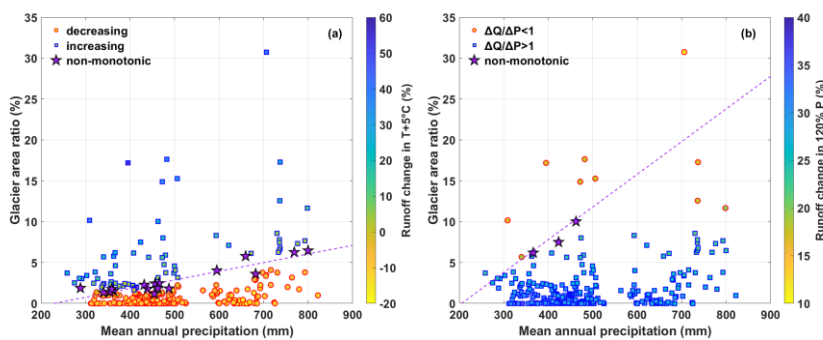
560

561 **Figure 9.** The correlations between the hydrological sensitivities to climate perturbation and
 562 the dominant influence factors.

563 On the contrary, the runoff change in response to increasing precipitation had a significant
 564 negative correlation ($r=-0.84, p<0.01$) with the GAR (Figure 9c), mainly due to the spatial
 565 variability of the runoff components. In REWs with larger GAR, the contribution of
 566 precipitation-induced runoff was relatively low due to the large contribution of glacier melt
 567 runoff, thus the influence of increasing precipitation on runoff change was also small. It should
 568 be noted that based on regression line in Figure 9c, the runoff change would be around zero in
 569 regions with GAR higher than 35, which was a rather surprising inference. This might be due
 570 to the small sample of REWs with high GAR based on current spatial discretization, resulting
 571 in the poor confidence in the end of the regression line. The runoff change in response to
 572 increasing temperature also negatively correlated with the MAP ($r=-0.42, p<0.01$, Figure 9d).
 573 The contribution of subsurface runoff component was higher in wetter conditions (Figure 6d),
 574 resulting in more evaporation and a lower runoff coefficient, which caused a relatively small

575 increase in runoff, similar with the finding by He et al. (2021b).

576 Our results indicate that the runoff in some REWs changed non-monotonically in response
577 to the increasing temperature. The characteristics of these non-monotonic REWs were further
578 analyzed. Interestingly, the GAR of non-monotonic REWs had a good linear relationship with
579 their MAP (Figure 10a). The regression equation of the linear relation was
580 $GAR(\%)=0.011*MAP(mm)-2.43$ ($r=0.92$). Moreover, this regression line was the dividing line
581 between the REWs where runoff increased with increasing temperature and those with opposite
582 runoff trends in the GAR-MAP plot (Figure 10a). The REWs located in the upper part of the
583 plot had larger runoff increasing rates. This indicated that the local hydrological sensitivity to
584 increasing temperature was determined by the relationship between GAR and MAP. In wetter
585 REWs with larger MAP, more glaciers were needed to offset the decreasing runoff due to the
586 increasing temperature and evaporation. These findings suggested the important role of glaciers
587 in determining the runoff change in response to climate change. Similar characteristics were
588 observed in the precipitation perturbation scenarios (Figure 10b). The runoff change rate was
589 different from the precipitation change rate in all REWs, and was consistently either higher or
590 lower than precipitation change rate in most REWs. But there were three REWs shifting from
591 $\Delta Q/\Delta P < 1$ to > 1 , the GAR and MAP of which also had linear relationship, forming the boundary
592 of REWs where runoff changed more significantly than precipitation and those with lower
593 runoff change rate. However, there were only three such non-monotonic REWs for precipitation
594 perturbation scenarios, providing less confidence to the boundary line. As a result, there were
595 some REWs lying lower than the boundary line but with lower runoff change rate than
596 precipitation (Figure 10b).



597

598 **Figure 10.** The interrelation among the REW scale glacier area ratio, mean annual
599 precipitation and the runoff change for (a) 5°C of warming and (b) 120% precipitation.

600 **4.2 Implications of the sensitivity analysis**

601 The sensitivity analysis indicated the important role of glaciers in providing meltwater to
602 offset the runoff decreasing caused by climate warming. Our study showed that glacier
603 meltwater had a limited contribution to the total runoff in the YTR basin, similar with some
604 recent studies (Wang et al., 2021; Cui et al., 2023), resulting in a decreasing runoff trend with
605 increasing temperature. However, the spatial pattern analysis indicated that the role of glacier
606 melt runoff could be rather significant in the regions with large area covered by glaciers. For
607 example, the runoff increased significantly in the Yangbajing tributary of the Lhasa River in
608 response to increasing temperature (Figure 8), consistent with previous research estimating a
609 high contribution of glacier melt to runoff in this region (Lin et al., 2020; Wang et al., 2023). It
610 is therefore necessary to address the spatial scale issue when discussing the role of glacier
611 meltwater on water resources.

612 Several studies have stressed the important role of glaciers on the TP as the largest global
613 store of frozen water which supplied freshwater resources to downstream regions (Yao et al.,
614 2022). This study quantitatively estimated the role of glacier meltwater in offsetting the
615 decreasing runoff with increasing temperature and evaporation. Our results indicated that the
616 influences of glacier on hydrological processes were highly dependent on the spatial scale and
617 the local meteorological characteristics. Specifically, the role of glacier meltwater would
618 undoubtedly be more significant in regions with larger glacier cover areas (Luo et al., 2018;
619 Zhao et al., 2019; Khanal et al., 2021). Meanwhile, the role of glaciers was smaller in wetter
620 regions with higher precipitation because of the relatively low contribution of glacier meltwater
621 in total runoff. Consequently, the regions with larger precipitation amounts but little glacier
622 coverage would face a greater risk of water resources shortage in a warming future (Figure 10a),
623 and other regions would face the similar condition because of the shrinking glacier area. Our
624 results also suggested a larger influence of precipitation change on runoff than that of
625 temperature change (Figure 4), thus an accurate projection of precipitation is crucial for the
626 assessment of water resources under climate change. Recent studies showed a decreasing

627 precipitation trend after 2000 in the YTR basin (Li et al., 2016; Luan and Zhai, 2022), likely
628 posing threats of water scarcity to the riparian regions and again highlighting the important role
629 of glacier in maintaining water resources.

630 Our results showed that the runoff responded to increasing temperature non-monotonically
631 in some regions. These non-monotonic REWs represented the most dynamic regions within the
632 basin, as they kept shifting between energy and water limited stages. Recent studies also
633 projected the non-monotonic runoff change on the TP at increasing warming levels (Cui et al.,
634 2023), i.e., the annual mean runoff for major rivers on the TP will significantly decrease by
635 0.1~3.2% at the warming level of 1.5°C, and increase by 1.5~12% at 3.0°C in the future.
636 Although seemingly similar, the two studies revealed two different phenomena. In particular,
637 the non-monotonic runoff change projected by Cui et al. (2023) was driven by the output put
638 of climatic projection data CMIP6 (Eyring et al., 2016), and the runoff change was dominated
639 by the tendencies and periodicities of climate factors, especially precipitation (Wu et al., 2022).
640 Our study analyzed the runoff change in response to climate warming with fixed precipitation
641 input, and the trend was the result of the comprehensive response of multiple water balance
642 components to climate change. The local non-monotonic hydrological sensitivity was
643 essentially a borderline condition of increasing and decreasing trend, which reflected the
644 balance of increasing meltwater and evaporation in response to climate warming.

645

646 **4.3 Limitations**

647 This study explored the sensitivities of hydrological processes to climate change by
648 designing temperature and precipitation perturbation scenarios, rather than projecting future
649 runoff using the forcing data from general circulation models (GCMs). The assumed climate
650 perturbation method is widely used in runoff projection studies (He et al., 2021b; Su et al., 2023;
651 Rasouli et al., 2014; Rasouli et al., 2015), with the advantage of avoiding the computation cost
652 of correcting biases and downscaling GCMs to regional scale (Piani et al., 2010; Xu et al.,
653 2019). However, the assumed climate perturbation did not reflect the gradual process of climate
654 change. Specifically, the temperature should go through relatively low warming levels before
655 arriving at the assumed highest level, but the climate perturbation method actually assumed an

656 abrupt climate change. Because of the relatively short simulation period, the potential trend
657 turning of meltwater caused by the combined effect of increasing melting rate and shrinking
658 glacier area cannot be reflected by the sensitivity analysis (Yao et al., 2022; Zhang et al., 2022a).
659 We can expect that the role of glaciers when temperature increases by 5°C in the future should
660 be less than our results, because the glacier covered area at that time will be less than the current
661 condition (Yao et al., 2022). Meanwhile, the potential influences of temperature and
662 precipitation change on soil and vegetation conditions (Boulanger et al., 2016) were not
663 considered when designing the climate perturbation scenarios. Besides, because climate
664 perturbation rather than climate ensemble was used to force the model, the representation of
665 uncertainties related to climate forcing was very simplified. Nonetheless, the simple sensitivity
666 analysis in this study helped better understand the separate effect of changing temperature and
667 precipitation on runoff, and informed the role of glaciers in controlling the spatial pattern of
668 runoff change.

669 Another limitation comes from the uncertainties of hydrological model. Although
670 validated by the measurement data of multiple objectives and several internal stations, the
671 model still had potential uncertainties. First, as the most important forcing data, the common
672 precipitation datasets in the YTR basin all had large uncertainties, due to the lack of validation
673 data in high elevation regions (Xu et al., 2017), leading to uncertainties in hydrological
674 simulation. The model underestimated the peak streamflow for most stations, which could be
675 attributed to the underestimated precipitation during wet seasons by CMFD dataset. Further
676 correction on the precipitation product based on more station data could be helpful to remove
677 the bias. Second, because of the complex hydrological processes and runoff components, the
678 parameter equifinality problem usually existed in the hydrological model in large mountainous
679 basins (Gupta et al., 2008; Nan et al., 2021a). He et al. (2019) indicated that the uncertainties
680 of runoff component contributions could be nearly 20% even when the simulations of
681 streamflow, snow, glacier and isotope were satisfied simultaneously. The misestimation of the
682 runoff regime would undoubtedly influence the sensitivity analysis. Third, the calibration
683 procedure of this work was rather simple, based on a combination of automatic algorithm and
684 manual selection. The influences of calibration scheme, optimized objective function (Gupta et
685 al., 2009; Majone et al., 2022) and the weights of multiple objectives (Tong et al., 2021) on

686 hydrological sensitivities were not analyzed deeply. For instance, different types of evaluation
687 metrics for multiple objectives were added together directly, which may result in different
688 impacts on the integrated objective function. Besides, the use of pySOT algorithm did not allow
689 for a comprehensive hydrological uncertainty analysis, because it aimed to achieve the best
690 fitness between observations and model outputs. Lastly, the calibrated parameters were
691 assumed to be spatially uniform within the whole basin to avoid introducing too many
692 parameters. Although this is similar to several large-scale modeling studies (e.g., Cui et al.,
693 2023; Lutz et al., 2014), the uniform parameter might be inadequate to represent the spatial
694 variability of hydrological processes, which may influence some conclusions of the sensitivity
695 analysis. For example, considering the potential spatial variability of glacier melting rate, the
696 characteristics of non-monotonic REWs in Figure 10 may not form a straight line. Currently
697 this work only considered the uncertainties introduced by natural climate variabilities. More
698 works are needed in the future to analyze the parameter sensitivities and the uncertainties from
699 calibration schemes.

700 **5. Conclusions**

701 This study adopted the tracer-aided hydrological model THREW-T in a typical large
702 mountainous basin Yarlung Tsangpo River (YTR) on the Tibetan Plateau (TP). The model was
703 validated against multiple objectives (streamflow, snow, glacier and isotope) and the
704 streamflow at internal stations. The sensitivities of hydrological processes to perturbed
705 temperature and precipitation were analyzed. The spatial pattern of local hydrological
706 sensitivities and the influence factors were explored. Our main findings are as follows:

707 (1) The THREW-T model performed well on simulating the streamflow, snow cover area
708 (SCA), glacier mass balance (GMB), and stream water isotope, ensuring good representation
709 of the key cryospheric processes and a reasonable estimation of the contributions of runoff
710 components. The model performed acceptably on simulating the streamflow at eight internal
711 stations located in the mainstream and two major tributaries, which indicated that the spatial
712 pattern of hydrological processes was reflected by the model, and provided confidence in the
713 sensitivity analysis.

714 (2) Most hydrological characteristics responded to increasing temperature and

715 precipitation oppositely. Increasing temperature led to decreasing annual runoff, SCA and GMB,
716 and changed the runoff variation showing a smaller inter-annual variation, a more even
717 distributed intra-annual distribution, and an earlier maximum runoff. It also influenced the
718 runoff regime by increasing the contributions of rainfall and glacier melt overland runoff, but
719 decreasing the subsurface runoff and snowmelt overland runoff. Increasing precipitation had
720 the opposite effects to increasing temperature.

721 (3) The distribution of local hydrological sensitivities had a strong spatial variability. The
722 local runoff change in response to increasing temperature varied significantly, with changing
723 rate of -18.6% to 54.3% for 5°C of warming. The glacier area ratio (GAR) was the dominant
724 factor of the spatial pattern of hydrological sensitivities to both perturbed temperature and
725 precipitation. Some regions had a non-monotonic runoff change rate in response to climate
726 perturbation, which represented the most dynamic regions within the basin, as they kept shifting
727 between energy and water limited stages. The GAR and mean annual precipitation (MAP) of
728 the non-monotonic regions had a linear relation, and formed the boundary of regions with
729 different runoff trends in the GAR-MAP plot.

730

731 **Code and data availability**

732 Code and data availability. The isotope data and the code of THREW-T model used in this study
733 are available from the corresponding author (tianfq@tsinghua.edu.cn). Other data sets are
734 publicly available as follows: DEM (<http://www.gscloud.cn/sources/details/310?pid=302>, last
735 access: 1 January 2019, Geospatial Data Cloud Site, 2019), CMFD
736 (<https://doi.org/10.11888/AtmosphericPhysics.tpe.249369.file>, Yang and He, 2019), glacier
737 inventory data (<https://doi.org/10.3972/glacier.001.2013.db>, Liu, 2012), glacier elevation
738 change data (<https://doi.org/10.6096/13>, Huggonet et al., 2021), NDVI
739 (<https://doi.org/10.5067/MODIS/MOD13A3.006>, Didan, 2015), LAI
740 (<https://doi.org/10.5067/MODIS/MOD15A2H.006>, Myneni et al., 2015), HWSD
741 (<https://data.tpdc.ac.cn/zh-hans/data/3519536a-d1e7-4ba1-8481-6a0b56637baf/?q=HWSD>,
742 last access: 1 January 2019, He, 2019). These datasets not publicly available are referred to in
743 the main text (Chen et al., 2018; Liu et al., 2007).

744

745 **Author contribution**

746 YN conceived the idea and collected data; YN and FT conducted analysis and wrote the paper.

747

748 **Financial support**

749 This study has been supported by the National Natural Science Foundation of China (grant no.
750 92047301) and the Shuimu Tsinghua Scholar Program.

751

752 **Competing interests**

753 At least one of the (co-)authors is a member of the editorial board of Hydrology and Earth
754 System Sciences.

755

756 **References**

757 Aygun, O., Kinnard, C., Campeau, S., and Krogh, S. A.: Shifting Hydrological Processes in a
758 Canadian Agroforested Catchment due to a Warmer and Wetter Climate, *Water*, 12,
759 10.3390/w12030739, 2020.

760 Bai, X. L., Zhao, W. Z., Liu, H., Zhang, Y. Y., Yang, Q. Y., Liu, J. T., and Chang, X. L.: Effects
761 of precipitation changes and land-use alteration on streamflow: A comparative analysis
762 from two adjacent catchments in the Qilian Mountains, arid northwestern China, *Frontiers*
763 in Environmental Science, 11, 10.3389/fenvs.2023.1097049, 2023.

764 Birkel, C. and Soulsby, C.: Advancing tracer-aided rainfall-runoff modelling: a review of
765 progress, problems and unrealised potential, *Hydrological Processes*, 29, 5227-5240,
766 10.1002/hyp.10594, 2015.

767 Bloschl, G. and Montanari, A.: Climate change impacts-throwing the dice?, *Hydrological*
768 *Processes*, 24, 374-381, 10.1002/hyp.7574, 2010.

769 Boulanger, Y., Taylor, A. R., Price, D. T., Cyr, D., McGarrigle, E., Rammer, W., Sainte-Marie,
770 G., Beaudoin, A., Guindon, L., and Mansuy, N.: Climate change impacts on forest
771 landscapes along the Canadian southern boreal forest transition zone, *Landscape Ecology*,

772 32, 1415-1431, 10.1007/s10980-016-0421-7, 2017.

773 Cao, L. G. and Pan, S. M.: Changes in precipitation extremes over the "Three-River
774 Headwaters" region, hinterland of the Tibetan Plateau, during 1960-2012, *Quaternary*
775 *International*, 321, 105-115, 10.1016/j.quaint.2013.12.041, 2014.

776 Chen, X., Long, D., Liang, S., He, L., Zeng, C., Hao, X., and Hong, Y.: Developing a composite
777 daily snow cover extent record over the Tibetan Plateau from 1981 to 2016 using
778 multisource data, *Remote Sensing of Environment*, 215, 284-299,
779 10.1016/j.rse.2018.06.021, 2018.

780 Criss, R. E. and Winston, W. E.: Do Nash values have value? Discussion and alternate proposals,
781 *Hydrological Processes*, 22, 2723-2725, 10.1002/hyp.7072, 2008.

782 Cui, T., Li, Y., Yang, L., Nan, Y., Li, K., Tudaji, M., Hu, H., Long, D., Shahid, M., Mubeen, A.,
783 He, Z., Yong, B., Lu, H., Li, C., Ni, G., Hu, C., and Tian, F.: Non-monotonic changes in
784 Asian Water Towers' streamflow at increasing warming levels, *Nature communications*,
785 14, 1176-1176, 10.1038/s41467-023-36804-6, 2023.

786 Didan, K.: MOD13A3 MODIS/Terra vegetation Indices Monthly L3 Global 1 km SIN Grid
787 V006, NASA EOSDIS Land Processes DAAC [dataset],
788 <https://doi.org/10.5067/MODIS/MOD13A3.006>, 2015.

789 Eriksson, D., Bindel, D., and Shoemaker, C. A.: pySOT and POAP: An event-driven
790 asynchronous framework for surrogate optimization, *arXiv preprint*,
791 10.48550/arXiv.1908.00420, 2019.

792 Eyring, V., Bony, S., Meehl, G. A., Senior, C. A., Stevens, B., Stouffer, R. J., and Taylor, K. E.:
793 Overview of the Coupled Model Intercomparison Project Phase 6 (CMIP6) experimental
794 design and organization, *Geoscientific Model Development*, 9, 1937-1958, 10.5194/gmd-
795 9-1937-2016, 2016.

796 Fassnacht, S. R., Sexstone, G. A., Kashipazha, A. H., Ignacio Lopez-Moreno, J., Jasinski, M.
797 F., Kampf, S. K., and Von Thaden, B. C.: Deriving snow-cover depletion curves for
798 different spatial scales from remote sensing and snow telemetry data, *Hydrological*
799 *Processes*, 30, 1708-1717, 10.1002/hyp.10730, 2016.

800 Fenicia, F., Kavetski, D., Reichert, P., and Albert, C.: Signature-Domain Calibration of
801 Hydrological Models Using Approximate Bayesian Computation: Empirical Analysis of

802 Fundamental Properties, *Water Resources Research*, 54, 3958-3987,
803 10.1002/2017wr021616, 2018.

804 Gao, J., Yao, T. D., Masson-Delmotte, V., Steen-Larsen, H. C., and Wang, W. C.: Collapsing
805 glaciers threaten Asia's water supplies, *Nature*, 565, 19-21, 10.1038/d41586-018-07838-4,
806 2019.

807 Gupta, H. V., Kling, H., Yilmaz, K. K., and Martinez, G. F.: Decomposition of the mean squared
808 error and NSE performance criteria: Implications for improving hydrological modelling,
809 *Journal of Hydrology*, 377, 80-91, 10.1016/j.jhydrol.2009.08.003, 2009.

810 Gupta, H. V., Wagener, T., and Liu, Y.: Reconciling theory with observations: elements of a
811 diagnostic approach to model evaluation, *Hydrological Processes*, 22, 3802-3813,
812 10.1002/hyp.6989, 2008.

813 He, Y.: Pan-TPE soil map based on Harmonized World Soil Database (V1.2), National Tibetan
814 Plateau Data Center [dataset], 2019.

815 He, Z. H. and Pomeroy, J. W.: Assessing hydrological sensitivity to future climate change over
816 the Canadian southern boreal forest, *Journal of Hydrology*, 624,
817 10.1016/j.jhydrol.2023.129897, 2023.

818 He, Z., Duethmann, D., and Tian, F.: A meta-analysis based review of quantifying the
819 contributions of runoff components to streamflow in glacierized basins, *Journal of*
820 *Hydrology*, 603, 10.1016/j.jhydrol.2021.126890, 2021a.

821 He, Z. H., Pomeroy, J. W., Fang, X., and Peterson, A.: Sensitivity analysis of hydrological
822 processes to perturbed climate in a southern boreal forest basin, *Journal of Hydrology*, 601,
823 10.1016/j.jhydrol.2021.126706, 2021b.

824 He, Z., Unger-Shayesteh, K., Vorogushyn, S., Weise, S. M., Kalashnikova, O., Gafurov, A.,
825 Duethmann, D., Barandun, M., and Merz, B.: Constraining hydrological model parameters
826 using water isotopic compositions in a glacierized basin, Central Asia, *Journal of*
827 *Hydrology*, 571, 332-348, 10.1016/j.jhydrol.2019.01.048, 2019.

828 Hindshaw, R. S., Tipper, E. T., Reynolds, B. C., Lemarchand, E., Wiederhold, J. G., Magnusson,
829 J., Bernasconi, S. M., Kretschmar, R., and Bourdon, B.: Hydrological control of stream
830 water chemistry in a glacial catchment (Damma Glacier, Switzerland), *Chemical Geology*,
831 285, 215-230, 10.1016/j.chemgeo.2011.04.012, 2011.

832 Hugonnet, R., McNabb, R., Berthier, E., Menounos, B., Nuth, C., Girod, L., Farinotti, D., Huss,
833 M., Dussailant, I., Brun, F., and Kaab, A.: Accelerated global glacier mass loss in the early
834 twenty-first century, *Nature*, 592, 726-+, 10.1038/s41586-021-03436-z, 2021.

835 Immerzeel, W. W., van Beek, L. P. H., and Bierkens, M. F. P.: Climate Change Will Affect the
836 Asian Water Towers, *Science*, 328, 1382-1385, 10.1126/science.1183188, 2010.

837 Jiang, Y., Xu, Z., and Xiong, L.: Runoff variation and response to precipitation on multi-spatial
838 and temporal scales in the southern Tibetan Plateau, *Journal of Hydrology-Regional
839 Studies*, 42, 10.1016/j.ejrh.2022.101157, 2022a.

840 Jiang, Y., Yang, K., Yang, H., Lu, H., Chen, Y., Zhou, X., Sun, J., Yang, Y., and Wang, Y.:
841 Characterizing basin-scale precipitation gradients in the Third Pole region using a high-
842 resolution atmospheric simulation-based dataset, *Hydrology and Earth System Sciences*,
843 26, 4587-4601, 10.5194/hess-26-4587-2022, 2022b.

844 Khanal, S., Lutz, A. F., Kraaijenbrink, P. D. A., van den Hurk, B., Yao, T., and Immerzeel, W.
845 W.: Variable 21st Century Climate Change Response for Rivers in High Mountain Asia at
846 Seasonal to Decadal Time Scales, *Water Resources Research*, 57, 10.1029/2020wr029266,
847 2021.

848 Li, X., Yao, Z., Xiao, J., and Wang, H.: Analysis of the spatial-temporal variation characteristics
849 of precipitation over the Tibetan Plateau from 1961 through 2010, *Journal of Glaciology
850 and Geocryology*, 38, 1233-1240, 2016.

851 Li, C., Sinha, E., Horton, D. E., Diffenbaugh, N. S., and Michalak, A. M.: Joint bias correction
852 of temperature and precipitation in climate model simulations, *Journal of Geophysical
853 Research-Atmospheres*, 119, 13153-13162, 10.1002/2014jd022514, 2014.

854 Li, Z. X., Feng, Q., Li, Z. J., Yuan, R. F., Gui, J., and Lv, Y. M.: Climate background, fact and
855 hydrological effect of multiphase water transformation in cold regions of the Western
856 China: A review, *Earth-Science Reviews*, 190, 33-57, 10.1016/j.earscirev.2018.12.004,
857 2019.

858 Li, Z. J., Li, Z. X., Song, L. L., Gui, J., Xue, J., Zhang, B. J., and Gao, W. D.: Hydrological and
859 runoff formation processes based on isotope tracing during ablation period in the source
860 regions of Yangtze River, *Hydrology and Earth System Sciences*, 24, 4169-4187,
861 10.5194/hess-24-4169-2020, 2020.

862 Li, K., Tian, F., Khan, M. Y. A., Xu, R., He, Z., Yang, L., Lu, H., and Ma, Y.: A high-accuracy
863 rainfall dataset by merging multiple satellites and dense gauges over the southern Tibetan
864 Plateau for 2014-2019 warm seasons, *Earth System Science Data*, 13, 5455-5467,
865 10.5194/essd-13-5455-2021, 2021.

866 Lin, L., Gao, M., Liu, J., Wang, J., Wang, S., Chen, X., and Liu, H.: Understanding the effects
867 of climate warming on streamflow and active groundwater storage in an alpine catchment:
868 the upper Lhasa River, *Hydrology and Earth System Sciences*, 24, 1145-1157,
869 10.5194/hess-24-1145-2020, 2020.

870 Liu, S.: The second glacier inventory dataset of China (version 1.0) (2006–2011), National
871 Tibetan Plateau Data Center [dataset], 10.3972/glacier.001.2013.db, 2012.

872 Liu, Z. F., Tian, L. D., Yao, T. D., Gong, T. L., Yin, C. L., and Yu, W. S.: Temporal and spatial
873 variations of delta O-18 in precipitation of the Yarlung Zangbo River Basin, *Journal of*
874 *Geographical Sciences*, 17, 317-326, 10.1007/s11442-007-0317-1, 2007.

875 Luan, L. and Zhai, P.: Changes in rainy season precipitation properties over the Qinghai-Tibet
876 Plateau based on multi-source datasets, *Progressus Inquisitiones de Mutatione Climatis*,
877 19, 173-190, 2023.

878 Luo, Y., Arnold, J., Liu, S., Wang, X., and Chen, X.: Inclusion of glacier processes for
879 distributed hydrological modeling at basin scale with application to a watershed in
880 Tianshan Mountains, northwest China, *Journal of Hydrology*, 477, 72-85,
881 10.1016/j.jhydrol.2012.11.005, 2013.

882 Luo, Y., Arnold, J., Liu, S. Y., Wang, X. Y., and Chen, X.: Inclusion of glacier processes for
883 distributed hydrological modeling at basin scale with application to a watershed in
884 Tianshan Mountains, northwest China, *Journal of Hydrology*, 477, 72-85,
885 10.1016/j.jhydrol.2012.11.005, 2013.

886 Luo, Y., Wang, X., Piao, S., Sun, L., Ciais, P., Zhang, Y., Ma, C., Gan, R., and He, C.:
887 Contrasting streamflow regimes induced by melting glaciers across the Tien Shan - Pamir
888 - North Karakoram, *Scientific Reports*, 8, 10.1038/s41598-018-34829-2, 2018.

889 Luo, Y., Wang, X. L., Piao, S. L., Sun, L., Ciais, P., Zhang, Y. Q., Ma, C. K., Gan, R., and He,
890 C. S.: Contrasting streamflow regimes induced by melting glaciers across the Tien Shan -
891 Pamir - North Karakoram, *Scientific Reports*, 8, 10.1038/s41598-018-34829-2, 2018.

892 Lutz, A. F., Immerzeel, W. W., Shrestha, A. B., and Bierkens, M. F. P.: Consistent increase in
893 High Asia's runoff due to increasing glacier melt and precipitation, *Nature Climate Change*,
894 4, 587-592, 10.1038/nclimate2237, 2014.

895 Majone, B., Avesani, D., Zulian, P., Fiori, A., and Bellin, A.: Analysis of high streamflow
896 extremes in climate change studies: how do we calibrate hydrological models?, *Hydrology
897 and Earth System Sciences*, 26, 3863-3883, 10.5194/hess-26-3863-2022, 2022.

898 McMillan, H., Westerberg, I., and Branger, F.: Five guidelines for selecting hydrological
899 signatures, *Hydrological Processes*, 31, 4757-4761, 10.1002/hyp.11300, 2017.

900 Moriasi, D. N., Arnold, J. G., Van Liew, M. W., Bingner, R. L., Harmel, R. D., and Veith, T. L.:
901 Model evaluation guidelines for systematic quantification of accuracy in watershed
902 simulations, *Transactions of the Asabe*, 50, 885-900, 10.13031/2013.23153, 2007.

903 Myneni, R., Knyazikhin, Y., and Park, T.: MOD15A2H MODIS/Terra Leaf Area Index/FPAR
904 8-Day L4 Global 500 m SIN Grid V006, NASA EOSDIS Land Processes DAAC [dataset],
905 10.5067/MODIS/MOD15A2H.006, 2015.

906 Nan, Y., Tian, F., Li, Z., and Gui, J.: Longer simulation time step of the tracer-aided hydrological
907 model estimates lower contribution of slow runoff components, *Journal of Hydrology*,
908 <https://doi.org/10.1016/j.jhydrol.2023.129889>, 2023.

909 Nan, Y., He, Z., Tian, F., Wei, Z., and Tian, L.: Can we use precipitation isotope outputs of
910 isotopic general circulation models to improve hydrological modeling in large
911 mountainous catchments on the Tibetan Plateau?, *Hydrology and Earth System Sciences*,
912 25, 6151-6172, 10.5194/hess-25-6151-2021, 2021a.

913 Nan, Y., He, Z., Tian, F., Wei, Z., and Tian, L.: Assessing the influence of water sampling
914 strategy on the performance of tracer-aided hydrological modeling in a mountainous basin
915 on the Tibetan Plateau, *Hydrology and Earth System Sciences*, 26, 4147-4167,
916 10.5194/hess-26-4147-2022, 2022.

917 Nan, Y., Tian, L., He, Z., Tian, F., and Shao, L.: The value of water isotope data on improving
918 process understanding in a glacierized catchment on the Tibetan Plateau, *Hydrology and
919 Earth System Sciences*, 25, 3653-3673, 10.5194/hess-25-3653-2021, 2021b.

920 Olsson, T., Jakkila, J., Veijalainen, N., Backman, L., Kaurola, J., and Vehvilainen, B.: Impacts
921 of climate change on temperature, precipitation and hydrology in Finland - studies using

922 bias corrected Regional Climate Model data, *Hydrology and Earth System Sciences*, 19,
923 3217-3238, 10.5194/hess-19-3217-2015, 2015.

924 Piani, C., Weedon, G. P., Best, M., Gomes, S. M., Viterbo, P., Hagemann, S., and Haerter, J. O.:
925 Statistical bias correction of global simulated daily precipitation and temperature for the
926 application of hydrological models, *Journal of Hydrology*, 395, 199-215,
927 10.1016/j.jhydrol.2010.10.024, 2010.

928 Rasouli, K., Pomeroy, J. W., and Marks, D. G.: Snowpack sensitivity to perturbed climate in a
929 cool mid-latitude mountain catchment, *Hydrological Processes*, 29, 3925-3940,
930 10.1002/hyp.10587, 2015.

931 Rasouli, K., Pomeroy, J. W., Janowicz, J. R., Carey, S. K., and Williams, T. J.: Hydrological
932 sensitivity of a northern mountain basin to climate change, *Hydrological Processes*, 28,
933 4191-4208, 10.1002/hyp.10244, 2014.

934 Reggiani, P., Hassanizadeh, S. M., Sivapalan, M., and Gray, W. G.: A unifying framework for
935 watershed thermodynamics: constitutive relationships, *Advances in Water Resources*, 23,
936 15-39, 10.1016/s0309-1708(99)00005-6, 1999.

937 Schaefli, B. and Gupta, H. V.: Do Nash values have value?, *Hydrological Processes*, 21, 99-
938 104, 2007.

939 Schaefli, B., Hingray, B., Niggli, M., and Musy, A.: A conceptual glacio-hydrological model
940 for high mountainous catchments, *Hydrology and Earth System Sciences*, 9, 95-109,
941 10.5194/hess-9-95-2005, 2005.

942 Stadnyk, T. A. and Holmes, T. L.: Large scale hydrologic and tracer aided modelling: A review,
943 *Journal of Hydrology*, 618, 10.1016/j.jhydrol.2023.129177, 2023.

944 Su, T., Miao, C. Y., Duan, Q. Y., Gou, J. J., Guo, X. Y., and Zhao, X.: Hydrological response to
945 climate change and human activities in the Three-River Source Region, *Hydrology and
946 Earth System Sciences*, 27, 1477-1492, 10.5194/hess-27-1477-2023, 2023.

947 Tang, Q. H., Lan, C., Su, F. G., Liu, X. C., Sun, H., Ding, J., Wang, L., Leng, G. Y., Zhang, Y.
948 Q., Sang, Y. F., Fang, H. Y., Zhang, S. F., Han, D. M., Liu, X. M., He, L., Xu, X. M., Tang,
949 Y., and Chen, D. L.: Streamflow change on the Qinghai-Tibet Plateau and its impacts,
950 *Chinese Science Bulletin-Chinese*, 64, 2807-2821, 10.1360/tb-2019-0141, 2019.

951 Tian, F., Hu, H., Lei, Z., and Sivapalan, M.: Extension of the Representative Elementary

952 Watershed approach for cold regions via explicit treatment of energy related processes,
953 Hydrology and Earth System Sciences, 10, 619-644, 10.5194/hess-10-619-2006, 2006.

954 Tian, F., Xu, R., Nan, Y., Li, K., and He, Z.: Quantification of runoff components in the Yarlung
955 Tsangpo River using a distributed hydrological model, *Advances in Water Science*, 31,
956 324-336, 2020.

957 Tong, R., Parajka, J., Salentini, A., Pfeil, I., Komma, J., Szeles, B., Kuban, M., Valent, P.,
958 Vreugdenhil, M., Wagner, W., and Bloeschl, G.: The value of ASCAT soil moisture and
959 MODIS snow cover data for calibrating a conceptual hydrologic model, *Hydrology and
960 Earth System Sciences*, 25, 1389-1410, 10.5194/hess-25-1389-2021, 2021.

961 van Pelt, S. C., Kabat, P., ter Maat, H. W., van den Hurk, B., and Weerts, A. H.: Discharge
962 simulations performed with a hydrological model using bias corrected regional climate
963 model input, *Hydrology and Earth System Sciences*, 13, 2387-2397, 10.5194/hess-13-
964 2387-2009, 2009.

965 van Pelt, S. C., Kabat, P., ter Maat, H. W., van den Hurk, B. J. J. M., and Weerts, A. H.:
966 Discharge simulations performed with a hydrological model using bias corrected regional
967 climate model input, *Hydrology and Earth System Sciences*, 13, 2387-2397, 10.5194/hess-
968 13-2387-2009, 2009.

969 Wang, S., Liu, J., Pritchard, H. D., Ke, L., Qiao, X., Zhang, J., Xiao, W., and Zhou, Y.:
970 Characterizing 4 decades of accelerated glacial mass loss in the west Nyainqentanglha
971 Range of the Tibetan Plateau, *Hydrology and Earth System Sciences*, 27, 933-952,
972 10.5194/hess-27-933-2023, 2023.

973 Wang, T., Zhao, Y. T., Xu, C. Y., Ciais, P., Liu, D., Yang, H., Piao, S. L., and Yao, T. D.:
974 Atmospheric dynamic constraints on Tibetan Plateau freshwater under Paris climate
975 targets, *Nature Climate Change*, 11, 10.1038/s41558-020-00974-8, 2021.

976 Wang, Y. W., Wang, L., Zhou, J., Yao, T. D., Yang, W., Zhong, X. Y., Liu, R. S., Hu, Z. D., Luo,
977 L., Ye, Q. H., Chen, N. S., and Ding, H. T.: Vanishing Glaciers at Southeast Tibetan Plateau
978 Have Not Offset the Declining Runoff at Yarlung Zangbo, *Geophysical Research Letters*,
979 48, 10.1029/2021gl094651, 2021.

980 Wang, L., Han, S., Tian, F., Li, K., Li, Y., Tudaji, M., Cao, X., Nan, Y., Cui, T., Zheng, X., Hu,
981 Z., Wang, W., and Yang, Y.: The Evaporation on the Tibetan Plateau Stops Increasing in

982 the Recent Two Decades, *Journal of Geophysical Research-Atmospheres*, 127,
983 10.1029/2022jd037377, 2022.

984 Wang, L., Yao, T. D., Chai, C. H., Cuo, L., Su, F. G., Zhang, F., Yao, Z. J., Zhang, Y. S., Li, X.
985 P., Qi, J., Hu, Z. D., Liu, J. S., and Wang, Y. W.: TP-River: Monitoring and Quantifying
986 Total River Runoff from the Third Pole, *Bulletin of the American Meteorological Society*,
987 102, E948-E965, 10.1175/bams-d-20-0207.1, 2021.

988 Wu, Y., Long, D., Lall, U., Scanlon, B. R., Tian, F., Fu, X., Zhao, J., Zhang, J., Wang, H., and
989 Hu, C.: Reconstructed eight-century streamflow in the Tibetan Plateau reveals contrasting
990 regional variability and strong nonstationarity, *Nature Communications*, 13,
991 10.1038/s41467-022-34221-9, 2022.

992 Xu, R., Hu, H. C., Tian, F. Q., Li, C., and Khan, M. Y. A.: Projected climate change impacts on
993 future streamflow of the Yarlung Tsangpo-Brahmaputra River, *Global and Planetary
994 Change*, 175, 144-159, 10.1016/j.gloplacha.2019.01.012, 2019.

995 Xu, R., Tian, F., Yang, L., Hu, H., Lu, H., and Hou, A.: Ground validation of GPM IMERG and
996 TRMM 3B42V7 rainfall products over southern Tibetan Plateau based on a high-density
997 rain gauge network, *Journal of Geophysical Research-Atmospheres*, 122, 910-924,
998 10.1002/2016jd025418, 2017.

999 Yang, K. and He, J.: China meteorological forcing dataset (1979–2018), National Tibetan
1000 Plateau Data Center [dataset], 10.11888/AtmosphericPhysics.tpe.249369.file, 2019.

1001 Yao, T. D.: Tackling on environmental changes in Tibetan Plateau with focus on water,
1002 ecosystem and adaptation, *Science Bulletin*, 64, 417-417, 10.1016/j.scib.2019.03.033,
1003 2019.

1004 Yao, Y. Y., Zheng, C. M., Andrews, C. B., Scanlon, B. R., Kuang, X. X., Zeng, Z. Z., Jeong, S.
1005 J., Lancia, M., Wu, Y. P., and Li, G. S.: Role of Groundwater in Sustaining Northern
1006 Himalayan Rivers, *Geophysical Research Letters*, 48, 10.1029/2020gl092354, 2021.

1007 Yao, T. D., Bolch, T., Chen, D. L., Gao, J., Immerzeel, W., Piao, S., Su, F. G., Thompson, L.,
1008 Wada, Y., Wang, L., Wang, T., Wu, G. J., Xu, B. Q., Yang, W., Zhang, G. Q., and Zhao, P.:
1009 The imbalance of the Asian water tower, *Nature Reviews Earth & Environment*, 3, 618-
1010 632, 10.1038/s43017-022-00299-4, 2022.

1011 Yoshimura, K., Kanamitsu, M., Noone, D., and Oki, T.: Historical isotope simulation using

1012 Reanalysis atmospheric data, *Journal of Geophysical Research-Atmospheres*, 113,
1013 10.1029/2008jd010074, 2008.

1014 Zhang, T., Li, D., East, A. E., Walling, D. E., Lane, S., Overeem, I., Beylich, A. A., Koppes, M.,
1015 and Lu, X.: Warming-driven erosion and sediment transport in cold regions, *Nature*
1016 *Reviews Earth & Environment*, 3, 832-851, 10.1038/s43017-022-00362-0, 2022a.

1017 Zhang, T., Li, D. F., and Lu, X. X.: Response of runoff components to climate change in the
1018 source-region of the Yellow River on the Tibetan plateau, *Hydrological Processes*, 36,
1019 10.1002/hyp.14633, 2022b.

1020 Zhang, F., Zhang, H. B., Hagen, S. C., Ye, M., Wang, D. B., Gui, D. W., Zeng, C., Tian, L. D.,
1021 and Liu, J. S.: Snow cover and runoff modelling in a high mountain catchment with scarce
1022 data: effects of temperature and precipitation parameters, *Hydrological Processes*, 29, 52-
1023 65, 10.1002/hyp.10125, 2015.

1024 Zhao, Q., Ding, Y., Wang, J., Gao, H., Zhang, S., Zhao, C., Xu, J., Han, H., and Shangguan, D.:
1025 Projecting climate change impacts on hydrological processes on the Tibetan Plateau with
1026 model calibration against the glacier inventory data and observed streamflow, *Journal of*
1027 *Hydrology*, 573, 60-81, 10.1016/j.jhydrol.2019.03.043, 2019.